UNIVERSITY OF CALIFORNIA SAN DIEGO

A Single-Cell Transcriptomic Profiling of the Effects of House Dust Mite Exposure on the Murine Lung Microenvironment

A Thesis submitted in partial satisfaction of the
requirements for the degree Master of Science

in

Biology

by

Han Chang

Committee in charge:

Professor Eyal Raz, Chair
Professor Matthew Daugherty, Co-Chair
Professor Cornelis Murre

2022

The thesis of Han Chang is approved, and it is acceptable in quality and form for publication on microfilm and electronically.

University of California San Diego

2022

TABLE OF CONTENTS

LIST OF FIGURES

LIST OF TABLES

ACKNOWLEDGEMENTS

I would like to acknowledge my PI, Eyal Raz, M.D., and my project mentor Samuel Bertin, Ph. D. for their guidance and support throughout my master's program. I also would like to acknowledge all the members of the Raz Lab for their support over the years I spent as an undergraduate and graduate student.

Figures 1, 2, and 3 are currently being prepared for submission for publication of the material. Wang, Dong-Jie; Chang, Han; Bertin, Samuel. "Chronic Exposure to House Dust Mites Accelerates Lung Cancer Progression in Mice by Activating the NLRP3/IL-1β Pathway in Lung Macrophages." The thesis author is a co-author of the materials.

ABSTRACT OF THE THESIS

A Single-Cell Transcriptomic Profiling of the Effects of House Dust Mite Exposure on the Murine Lung Microenvironment

by

Han Chang

Master of Science in Biology

University of California San Diego, 2022

Professor Eyal Raz, Chair
Professor Matthew Daugherty, Co-Chair

House Dust Mite (HDM) is a common aeroallergen that can induce allergic airway inflammation and asthma. The effects of acute exposure to HDM have been well studied in various mouse models of asthma; however, the effects of chronic exposure have been much less investigated. Our studies identified that chronic exposure to HDM induces chronic lung inflammation and accelerates lung cancer development in two different mouse models of lung cancer. The lung cancer-promoting effect of HDM was mainly due to chronic activation of the NLRP3 inflammasome in lung macrophages and persistent production of IL-1β in the lungs. Based on these findings, we hypothesize that chronic exposure to HDM changes the lung microenvironment and makes it conducive to tumor growth by activating the IL-1β signaling

pathway. To further evaluate the mechanisms by which HDM affects the lung microenvironment, we conducted a single-cell RNA sequencing (scRNA-seq) analysis and compared the effect of chronic HDM exposure in the lungs of wild-type (WT) and IL-1β knockout (KO) mice. Our findings suggest that HDM exposure and IL-1β signaling affect various immune cell types in the lungs such as macrophages, neutrophils, B cells, and T cells, which may contribute to the protumorigenic effects of HDM via IL-1β signaling pathway. Our study revealed a novel view of the transcriptomic landscape of the murine lung and uncovered novel effects of chronic HDM exposure and IL-1β signaling on the lung microenvironment.

INTRODUCTION

Lung Cancer

Lung cancer is the leading cause of all cancer-related death worldwide and accounts for roughly 1.9 million deaths every year [1]. One well-known risk factor for lung cancer is tobacco smoking, yet 25% of lung cancer cases are diagnosed in non-smokers [2]. Non-smoker cases of lung cancer have been attributed to other risk factors including exposure to radon gas, asbestos, air pollution, or genetic factors [2]. Chronic lung diseases and persistent lung inflammation also contribute to lung cancer development in non-smokers [3]. However, the exact mechanisms by which chronic lung inflammation promotes lung cancer remain unclear.

Chronic Lung Inflammation and Lung Cancer

The association between chronic inflammation and cancer is a long-established clinical observation [4]. Inflammation is a biological defense response to harmful agents during which inflammatory mediators such as cytokines, chemokines, and reactive oxygen species are released by immune cells [5]. While acute inflammation lasts only a few days with symptoms of redness or swelling, chronic inflammation is a slow and long-term process. In chronic inflammation, continuous infiltration of primary inflammatory cells is accompanied by the production of inflammatory mediators. These inflammatory mediators may contribute to tumorigenesis by supporting tumor-inducing epigenetic alteration and silencing tumor suppressor genes, and thus facilitate all stages of tumor development, including tumor initiation, tumor progression, invasion, and metastasis [7]. Chronic inflammation may also induce an immunosuppressive tumor microenvironment (TME) conducive to tumor growth and progression [7]. Due to its protumorigenic effects, chronic inflammation is considered to be a major risk factor for many

cancers. In fact, many chronic inflammatory diseases are positively correlated with the risk of cancer. For instance, chronic intestinal inflammation as occurring in inflammatory bowel disease is an established risk factor for colorectal cancer and gastrointestinal malignancy [8]. Likewise, chronic inflammatory lung diseases could potentially promote lung tumor initiation and lung cancer. There is strong evidence that chronic obstructive pulmonary disorder (COPD), a chronic inflammatory lung disease mainly caused by cigarette smoking, is a risk factor for lung cancer [9]. However, the positive association between other chronic inflammatory lung diseases and the risk of lung cancer is not clear.

Asthma and Lung Cancer

Allergic asthma is one of the most common chronic inflammatory lung diseases affecting 10-15% of western populations [10]. Asthma is characterized by airway inflammation, airway hyperresponsiveness (AHR), and smooth muscle remodeling. It is an heterogenous disease with different severities and symptoms but it can be classified into two main endotypes: T helper 2 (Th2) type or T helper 17 (Th17) type [11]. The Th2 endotype expresses high level of Th2 cells which produce Th-2 cytokines such as IL-4, IL-5, and IL-13 and consequently result in eosinophilic inflammation [12]. Another endotype expresses Th17 cells, producing IL-17A and IL-17F and leading to neutrophilic inflammation [12]. Due to the wide range of heterogeneity and severity of allergic asthma, it is not surprising that epidemiological studies on the relationship between asthma and lung cancer have been controversial. A meta-regression and meta-analysis conducted by Rosenberger *et al.* suggested that there was no causal relationship between asthma and lung cancer [13]. On the other hand, meta-analysis studies conducted by Qu et al. and Brown et al. suggested the positive correlation of asthma with lung cancer development [14, 15]. Furthermore, the

comprehensive cohort study from 2002 to 2015 conducted in South Korea by Woo *et al.* showed that adults with allergic asthma had a 75% greater risk of overall cancer and 2.8-fold increased risk of lung cancer, yet asthma patients taking high doses of inhaled corticosteroid, an anti-inflammatory medication, showed 56% reduced risk of lung cancer [16]. This study thus suggests that chronic inflammation in allergic asthma may contribute to lung cancer development. However, the positive association between asthma and lung cancer is presently inconclusive due to the conflicting epidemiological studies. Hence, the link between asthma and lung cancer remains controversial and the molecular mechanism by which asthma may increase the risk of lung cancer is still unknown. Therefore, additional studies are needed to further evaluate the potential link between asthma and lung cancer.

House Dust Mites (HDM)

HDM extracts (*Dermatophagoides* species) are widely used in allergic asthma models in mice because ~85% of asthmatics are allergic to HDM [17]. HDM are one of the most common indoor aeroallergens in the world, which can be found in carpets, clothes, and beds as well as public transportation. HDM are microscopic insects with a complex mixture of multiple digestive enzymes and microbial products such as lipopolysaccharide (LPS) and chitin, a component of the mite exoskeleton [17]. This mixture of bioactive molecules can provoke severe lung inflammation, airway hypersensitiveness (AHR), airway remodeling, and thus allergic asthma in both mice and humans [17, 18]. Because HDM and its bioactive molecules have multiple pathogen-associated molecular patterns (PAMPs) and allergenic epitopes, chronic HDM inhalation induces a mixed Th2 and Th17 immune response in the lungs with increased macrophage, neutrophil, and eosinophil recruitment, causing airway inflammation and subsequently airway remodeling [17, 18].

Thus, HDM could potentially change the lung microenvironment, making the lungs a conducive environment for tumor growth by stimulating the secretion of pro-inflammatory cytokines such as interleukin-1β (IL-1β) [18].

IL-1β

IL-1β is one of the pro-inflammatory cytokines that contribute to asthma exacerbation [19]. Upon infection, the activation of PAMPs such as LPS upregulates the expression of both NLRP3 (NOD-, LRR- and pyrin domain-containing protein 3) and pro-IL-1β in macrophages [20]. Then, both PAMPs and damage-associated molecular patterns (DAMPs) such as particulates, mitochondrial dysfunction, or lysosomal rupture, can trigger NLRP3 oligomerization and form NLRP3 inflammasome, which is a cytosolic multiprotein complex [21]. Activated NLRP3 inflammasome cleaves pro-caspase-1 into active caspase-1, which in turn cleaves pro-IL-1β into mature IL-1β [22]. IL-1β is known to be involved in Th2 and Th17 responses upon HDM exposure, inducing AHR and tissue remodeling in both mice and humans [23]. In addition, many asthmatic patients express a high level of IL-1β production [24]. As more recent findings suggested that IL-1β can induce carcinogenesis or mediate angiogenesis and metastasis [25], we hypothesized that chronic exposure to HDM constantly activates the NLRP3 inflammasome and significantly upregulate IL-1β production in the lungs, thus potentially promoting lung cancer development.

Single-cell RNA Sequencing (scRNA-seq)

Due to the complexity of constituents of HDM and its complicated consequences on both adaptive and innate host immunity, we assumed that scRNA-seq would be an ideal experimental tool to evaluate the comprehensive effects of chronic HDM exposure in the lungs. scRNA-seq

provides molecular profiles of each individual cell, thus allowing unbiased quantitative characterization of cellular heterogeneity [27]. As more than 40 different cell types are present in the lungs [27], scRNA-seq analysis appears as a technique of choice to identify the changes in lung cell subpopulations induced by chronic HDM exposure. We further sought to evaluate whether the effect of HDM on lung cell subpopulations was dependent on the IL-1β signaling pathway by comparing the data generated in WT mice with those in IL-1β KO mice. We first identified the transcriptomic profiling of various cell types present in the murine lung microenvironment exposed to HDM either in the presence or absence of IL-1β. We then analyzed whether the altered cell subpopulations or modulated gene expression within a subpopulation by HDM could support our findings generated in the lung cancer models and be associated with tumor development.

Working Hypothesis

We hypothesized that chronic exposure to HDM promotes lung cancer in susceptible hosts (i.e., mice or potentially humans genetically predisposed to lung cancer or co-exposed to lung carcinogens) by changing the lung microenvironment and making it conducive to tumor growth by activating the IL-1β signaling pathway.

METHODS

Mice

Young adult (2 to 6 months) WT C57BL/6 mice were initially purchased from the Jackson laboratory (JAX). Initial breeding pairs of IL-1β KO mice on the C57BL/6 background (JAX strain # 034447) was a gift from Dr. Wai Wilson Dr. Cheung Robert, and Dr. Hal Hoffman (all from UCSD). Initial breeding pairs of $CCSP^{Cre}$ [28] and $Kras^{G12D}$ [29] on the C57BL/6 background were a gift from Dr. Seon Hee Chang (The University of Texas MD Anderson Cancer Center). The resulting $CCSP^{Cre+/-}$ $Kras^{G12D+/-}$ were generated in our lab by crossing $Kras^{G12D}$ flox/flox mice with Club cell (formerly Clara cell) secretory protein (CCSP) cre+ mice in order to specifically induce $Kras^{G12D}$ expression in Club cells. All the mice were bred in our vivarium under standard conditions (e.g., 12-hour light and 12-hour dark cycle, standard chow diet, and water). All experimental procedures performed on mice were approved by the University of California San Diego Institutional Animal Care and Use Committee.

In vivo experimental procedures

Age- and sex-matched mice were treated intranasally (i.n) with the control vehicle (VEH; normal saline), HDM (*Dermatophagoides pteronyssinus*, Greer laboratories # XPB82D3A2.5), or heat-inactivated HDM (HI-HDM; 1h at 95ºC) under general anesthesia (isoflurane). Below are the specific protocols for each in vivo experiment.

- *Model 1: Kras-induced lung cancer model*

Age- and sex-matched Kras mice were first sensitized with 50 μg/mouse of HDM or HI-HDM, or an equivalent volume (30 μL) of VEH on day 0 and subsequently challenged with 12.5 μg/mouse of HDM or HI-HDM, or VEH twice per week for the first 4 weeks, and once per week for next 4

weeks (Fig. 1A). 13 weeks after the first i.n. treatment, the bronchoalveolar lavage fluid (BALF) was collected following standard procedures in a total 1.4 mL of PBS and the lungs were harvested. After ligation, one lung lobe of the right lung was removed, snap-frozen in liquid nitrogen, and stored at - 80°C until further processing. The remaining 4 lung lobes were fixed by intratracheal instillation and immersion fixed in 10% buffered formalin solution for 24h and were transferred to 70% ethanol until paraffin embedding. 4-6-μm mouse lung FFPE sections were stained with hematoxylin and eosin (H&E) and evaluated for the occurrence of lung tumors.

- *Model 2: Kras-induced lung cancer model with anti-IL1β or anti-CCL2 antibodies*

Another cohort of Kras mice was treated i.n. with VEH or HDM for 9 weeks as in model 1, but also injected intraperitoneally (i.p.) with 50 μg/mouse of anti-IL-1β, anti-CCL2 or with the isotype control (ctrl) antibody (Ab) 1h before each VEH or HDM i.n treatment and then, once a week during the last 4 weeks (Fig. 2A). 13 weeks after the first i.n. treatment the lungs were harvested and processed as indicated above.

- *Model 3: Urethane-induced lung cancer model*

Age- and sex-matched C57BL/6 WT or IL-1β KO mice were sensitized with 50 μg /mouse of HDM or with 50 μL/mouse VEH on day 0 and challenged i.n as depicted in Fig. 3A. During the 10 weeks of HDM challenge, the mice were injected i.p. with urethane (Sigma # U2500; 1 mg/g of BW) once a week (Fig. 3A). 26 weeks after the first urethane injection, the mice were sacrificed and the occurrence of lung tumors was evaluated on H&E-stained lung sections as indicated above.

- *Model 4: HDM-induced chronic lung inflammation model for scRNA-seq analysis*

Age-matched male C57BL/6 WT or IL-1β KO mice were sensitized with 50 μg/mouse of HDM or with 50 μL/mouse VEH on day 0 and challenged i.n three times a week for the subsequent 4 weeks with HDM (12.5 μg/mouse) or with VEH (50 μL/mouse). Mice were last challenged with

HDM or VEH on day 35 and were sacrificed 24 hours after the last HDM challenge. The lungs were harvested, and single-cell suspensions were prepared as described below.

Histopathological analysis

H&E-stained lung sections were scanned on an AT2 Aperio Scan Scope (Leica Biosystems). The digitalized images were analyzed using QuPath Software to calculate the tumor multiplicity (i.e., the number of lung tumors). The images were reviewed by a pathologist who was blinded to the procedures.

Enzyme-linked immunosorbent assay (ELISA)

CCL2 levels in the BALF samples were obtained using appropriate ELISA kits from eBioscience and following the manufacturers' instructions.

Statistical analysis

GraphPad Prism software was used to compute the statistics. For data with 2 groups, unpaired student's t-tests with two-tailed p-values were used. The statistical significance between more than two groups was determined using one- or two-way ANOVA with post hoc Bonferroni's test.

Single-Cell Suspensions and FACS sorting for scRNA-seq

Mice lungs were perfused by cardiac perfusion with 5 mL HBSS/1mM EDTA. Five lung lobes/mouse were harvested, manually minced with scissors, and then enzymatically digested in 2 mL of digestion buffer (500 μL Collagenase IA (Sigma Cat No: C9891), 100 μL DNAse I Type IV (Sigma Cat No: D5025), 250 uL Penicillin-Streptomycin (Sigma Cat No: P4333), and 5% FCS.

RBCs were lysed using ACK buffer (0.5 mL, 1 minute on ice), filtered through a 40 μm filter, and single-cell suspensions from n = 3-4 mice/group were pooled together. The cells were resuspended in PBS/2% FCS, stained using Annexin V-PE and DAPI, and sorted on a BD FACS Aria cell sorter (BD Biosciences) to remove transcriptional noise from dead/dying cells. Live single cells (Annexin V and DAPI double negative) were counted, resuspended in PBS/0.04% BSA, and processed immediately for scRNA-seq as indicated below.

Single-Cell Library Preparation and Sequencing

A total 16,500 cells per sample were loaded in duplicate on the Chromium Controller using the Single Cell 3' kit v3.1 Dual Index (10X Genomics # 1000268) for a desired 10,000-target cell recovery (Fig. 6B, C). Four samples were loaded in duplicate on a 10X chip for Gel beads-in-Emulsions (GEM) generation. Barcoding, post GEM-RT clean up, cDNA amplification, and library construction were conducted according to the manufacturer's instructions in the IGM Genomics Center at UC San Diego funded by the National Institutes of Health SIG grant #S10 OD026929. After post-library QC on an Agilent High Sensitivity D1000 Screentape, Illumina NovaSeq 6000 S4 was used for high-throughput sequencing of the samples, yielding about 200 million reads per sample.

Single-cell Analysis

The reads were demultiplexed, subsequently aligned to the murine reference genome (mm10-2020-A), filtered, and quantified by CellRanger 5.0.1 (10X Genomics). All samples had high-quality reads (Q30 > 90%) and excellent mapping rates to the genome (~95%). R package Seurat [30] was used to preprocess and analyze the sequencing data. Initial 61949 cells were filtered by

the number of genes and mitochondrial gene percentage to remove outliers such as dying cells, doublet, or multiplets as recommended by Seurat developers. After filtering, the counts of 55,050 cells were log-normalized to identify 2,000 highly variable genes for downstream analysis by FindVariableFeatures command in Seurat.

Clustering and Identification of Cell Types

PCA was carried out on the integrated data of 2,000 highly variable genes from all samples by Seurat commands with the set seed of 7 for reproducibility. UMAP was then conducted with a resolution of 0.3 for visualization and clustering of the cells, yielding initial 22 clusters. Differential gene expression for each cluster was identified by Seurat FindConservedMarkers function. The identity of each cluster was predicted based on known cell type markers from published studies, SingleR package, GeneCard and ImmGen database. The clusters of similar or identical cell types were merged together, yielding 11 clusters from the initial 21 clusters.

RESULTS

Chronic exposure to HDM accelerates lung cancer development by activating the NLRP3/IL-1β signaling pathway in lung macrophages

We first used a genetically driven model with oncogenic Kras activation in lung epithelial cells, the $CCSP^{Cre+/-}$ $K\text{-}ras^{G12D+/-}$ mouse (hereafter referred to as Kras mice) [29, 31]. We treated age- and sex-matched Kras mice intranasally (i.n) with HDM, heat-inactivated HDM (HI-HDM), or the control vehicle (VEH; normal saline) under light anesthesia (isoflurane) and evaluated the occurrence of lung tumors 13 weeks after the first i.n treatment (Fig. 1A). Histopathological evaluation of lung sections stained with hematoxylin and eosin (H&E) revealed that Kras mice treated with HDM had a significantly increased number of lung tumors as compared to VEH-treated mice, and to a lesser degree with HI-HDM (Fig. 1B, C), suggesting that chronic exposure to HDM promotes tumor development and that heat-sensitive factors in HDM extracts (e.g., proteolytic enzymes derived from the mite's digestive system) contribute to this effect.

Recent studies suggest that chronic activation of the NLRP3 inflammasome and the resulting increase in IL-1β production are associated with tumor progression in various types of cancer, including lung cancer [32, 33]. Thus, we evaluated the potential activation of this signaling pathway in the lungs of Kras mice treated with VEH, HDM, or HI-HDM. By doing western blot analysis of the homogenized lung tissues, we detected a strong increase in NLRP3 expression, caspase 1 cleavage, and production of mature IL-1β in the lungs of Kras mice treated with HDM, and to a lesser extent in those of mice treated with HI-HDM (Fig. 1E), as compared to VEH-treated mice. Because macrophages are one of the major cell types that express NLRP3 and produce IL-1β [34, 35], we next determined the expression of CCL2, a main inflammatory chemokine attracting primarily monocytes to sites of inflammation and inducing their differentiation into

macrophages [36], in the bronchoalveolar lavage fluid (BALF) of Kras mice from the three different experimental groups. In this model, CCL2 level in the BALF was found to correlate with increased macrophage numbers and with lung tumor development [37]. In agreement with this study, we observed an increased CCL2 production in the BALF of Kras mice treated with HDM compared to those of VEH- or HI-HDM-treated mice (Fig. 1D). Previous in vitro assays in the lab in which I did not participate identified that HDM concentration-dependently stimulated IL-1β production by bone marrow-derived macrophages (BMDMs) and by the RAW 264.7 mouse macrophage-like cell line (data not shown). Previous flow cytometry assays also demonstrated that lung macrophages recovered from HDM-treated Kras mice express higher intracellular levels of pro-IL-1β than those from VEH-treated mice (data not shown). Collectively, these data suggest that chronic i.n instillation of HDM may promote lung cancer development by activating the NLRP3/IL-1β signaling pathway in lung macrophages.

Neutralization of either IL-1β or CCL2 inhibited the lung cancer-promoting effect of HDM in Kras mice

Next, we treated another cohort of Kras mice i.n with HDM or VEH and i.p with a neutralizing antibody (Ab) against IL-1β or CCL2, or with the isotype control Ab, and determined the occurrence of lung tumors in the six experimental groups (Fig. 2A). As previously reported by others, IL-1β neutralization did not affect spontaneous tumor formation in Kras mice [38] as the tumor multiplicity was similar in mice treated with VEH and anti-IL-1β Ab, and in mice treated with VEH and isotype control Ab (Fig. 2B, C). However, IL-1β neutralization almost completely abolished the lung cancer-promoting effect of HDM (Fig. 2B, C). CCL2 neutralization slightly decreased spontaneous tumor formation in Kras mice (Fig. 2B, C). Furthermore, as observed for

IL-1β blockade, CCL2 neutralization almost completely abolished the lung cancer-promoting effect of HDM (Fig. 2B, C).

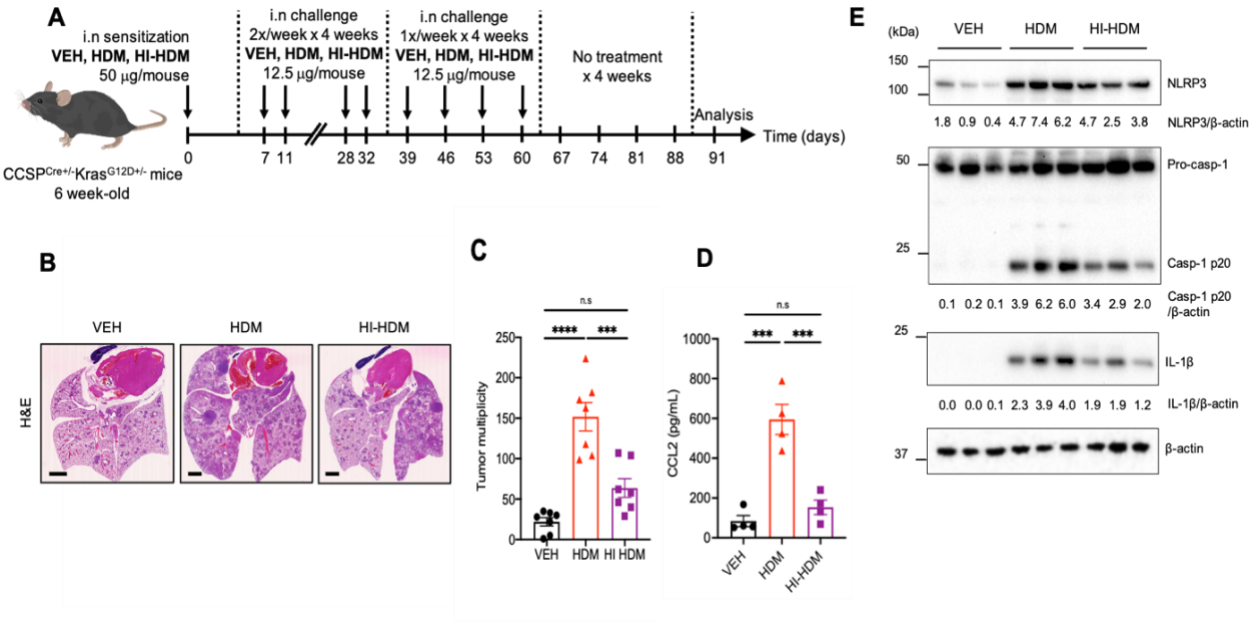

Figure. 1. Chronic HDM inhalation accelerated LC and activated the NLRP3/IL-1β pathway in the lungs of Kras mice. A) CCSP^{Cre}/K-ras^{G12D} (Kras) mice were treated from 5 to 18 weeks of age intranasally (i.n) with the VEH, HDM, or HI-HDM (n = 7 mice/group) as described in this schematic overview of the study design. **B)** Representative pictures of hematoxylin and eosin (H&E)-stained lung sections. Scale bars, 2 mm. **C**) The tumor multiplicity (i.e., number of lung lesions on 4 lung lobes per mouse) was determined on H&E-stained sections using QuPath software. **D)** ELISA analysis of CCL2 production in BALF recovered from Kras mice from the three different groups (n = 4 mice/group). **E)** Western blot analysis of NLRP3, Casp-1 p20, and IL-1β expression in homogenized lung tissues (n = 3 mice/group). ImageJ software was used for the densitometry analysis, and the band intensities were normalized to β-actin expression as indicated by the numbers below each blot. Data are expressed as mean ± SEM. n.s: not significant, *** $P < 0.001$, **** $P < 0.0001$ (one-way ANOVA with post hoc Bonferroni's test). Figure 1 is currently being prepared for submission for publication of the material. Wang, Dong-Jie; Chang, Han; Bertin, Samuel. "Chronic Exposure to House Dust Mites Accelerates Lung Cancer Progression in Mice by Activating the NLRP3/IL-1β Pathway in Lung Macrophages." The thesis author is a co-author of the materials.

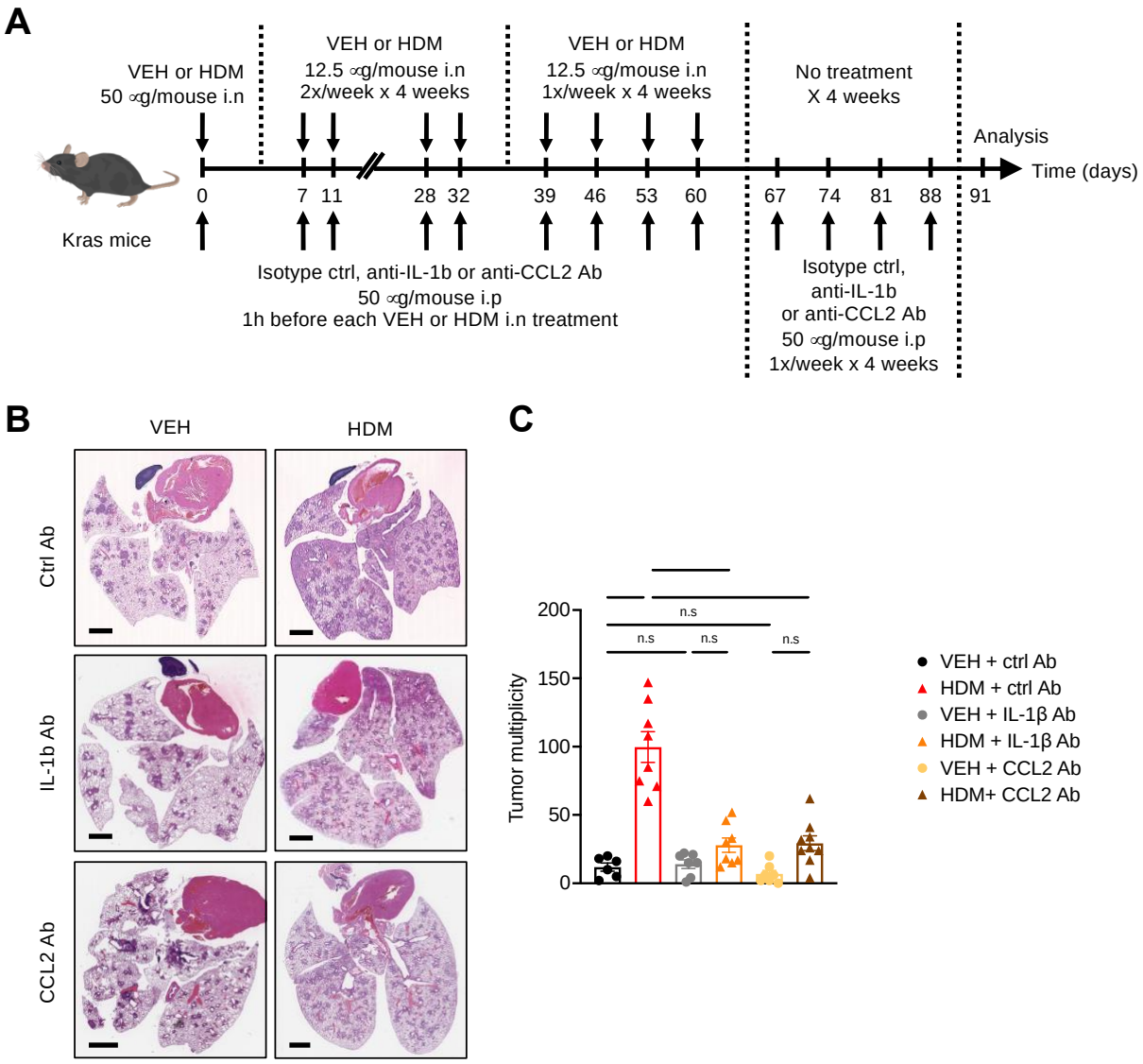

Figure 2. Effects of neutralizing antibodies against IL-1β or CCL2 in Kras mice treated with VEH or HDM. A) Five-week-old Kras mice were randomly assigned to six groups and were treated i.n with VEH or HDM and i.p with a neutralizing anti-IL-1β, anti-CCL2 or with the isotype control (ctrl) antibody (Ab) as indicated. **B)** Representative pictures of H&E-stained lung sections of mice in the six experimental groups. Scale bars, 2 mm. **C)** Tumor multiplicity (i.e., number of lung lesions per mouse) was calculated on H&E-stained sections as shown in B. Data are representative of one (CCL2 Ab) or two (IL-1β Ab) independent experiments and are expressed as mean ± SEM. VEH + ctrl Ab (n = 6), HDM + ctrl Ab (n = 8), VEH + IL-1β Ab (n = 7), and HDM + IL-1β Ab (n = 8), VEH + CCL2 Ab (n = 7), and HDM + CCL2 Ab (n = 9). n.s: not significant, * $P < 0.05$, ** $P < 0.01$, *** $P < 0.001$, **** $P < 0.0001$ (one-way ANOVA with post hoc Bonferroni's test). Figure 2 is currently being prepared for submission for publication of the material. Wang, Dong-Jie; Chang, Han; Bertin, Samuel. "Chronic Exposure to House Dust Mites Accelerates Lung Cancer Progression in Mice by Activating the NLRP3/IL-1β Pathway in Lung Macrophages." The thesis author is a co-author of the materials.

Chronic exposure to HDM accelerates lung cancer development in a urethane-induced lung cancer model and IL-1β neutralization inhibits this effect

We next evaluate the effect of chronic HDM exposure and IL-1β blockade in the urethane-induced lung cancer model [39, 40]. We employed a previously established two-stage lung carcinogenesis protocol, which consisted of ten weekly i.p. injections (tumor initiation stage) of urethane followed by a 16 week resting period (tumor promotion stage). This protocol was shown to overcome the resistance of C57BL/6 mice to lung carcinogenesis and caused a nearly 100% lung tumor incidence [41]. We treated wild-type (WT) and IL-1β KO C57BL/6 mice i.p with urethane and i.n with HDM or VEH (Fig. 3A). Consistent with our findings in Kras mice, WT mice treated with urethane and HDM showed increased tumor multiplicity compared to WT mice treated with urethane and VEH (Fig. 3B, C). Furthermore, in line with the effect of IL-1β neutralization in Kras mice, the tumor multiplicity was strongly reduced in IL-1β KO mice treated with urethane and HDM as compared to WT mice that received the same treatments (Fig. 3B, C). We obtained similar results in caspase-1/11 KO mice treated with urethane and with HDM or VEH (data not shown). We are also currently treating CCL2 KO mice with VEH or HDM and urethane but because of the long duration of this model (approximatively 7 months), we won't have the results on time to include them in this thesis.

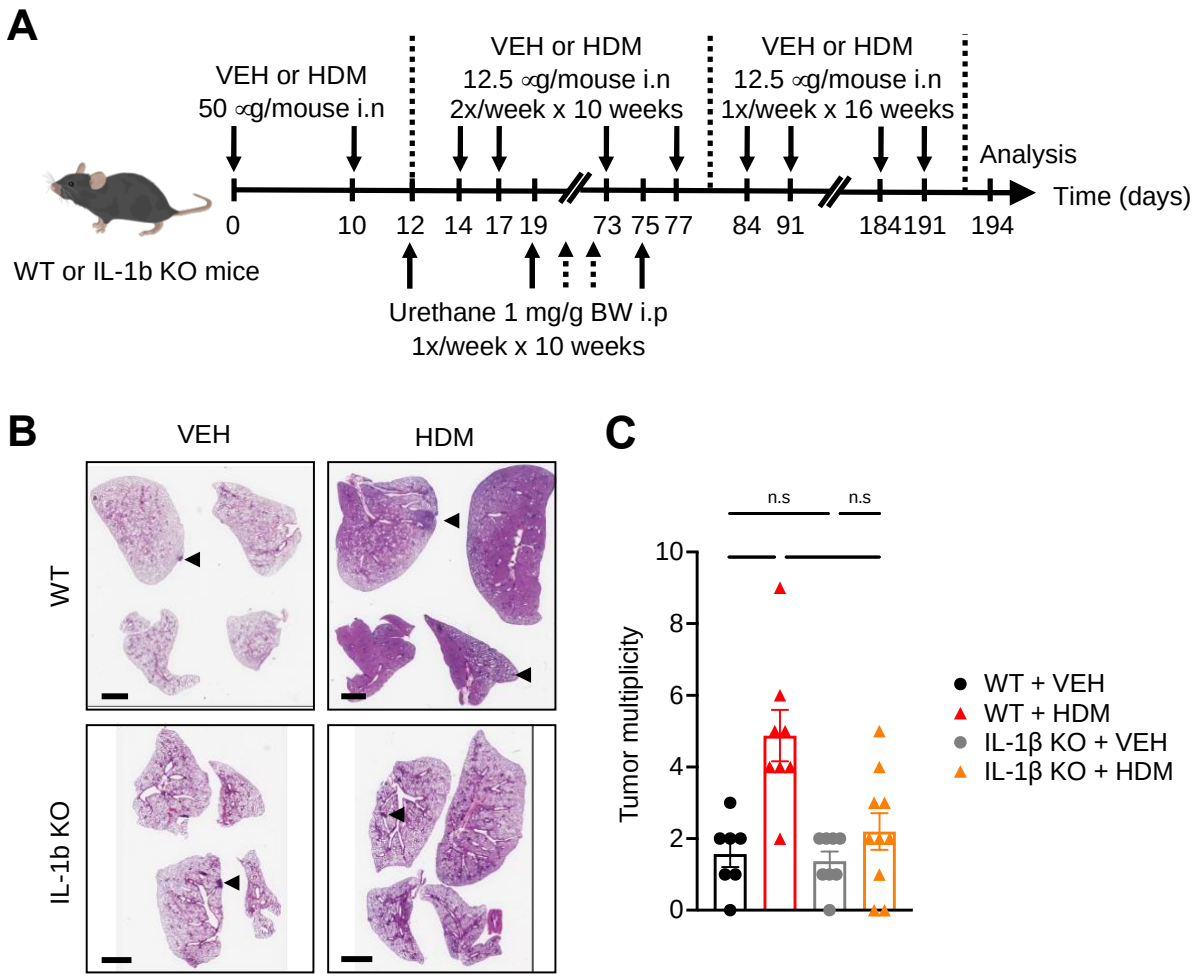

Figure 3. IL-1β neutralization inhibits the lung tumor-promoting effect of HDM in the urethane-induced lung cancer model. A) Age- and sex-matched WT and IL-1β KO C57BL/6 mice were treated i.n with VEH or HDM and with urethane as indicated in this schematic overview of the study design. **B)** Representative pictures of H&E-stained lung sections of mice in the four experimental groups. Four lobes per mouse are shown. Arrow heads indicate tumors. Scale bars, 1 mm. **C)** Tumor multiplicity (i.e., number of lung lesions per mouse) was calculated on H&E-stained sections as shown in B. Data are representative of two independent experiments and are expressed as mean ± SEM of 6-10 mice per group. WT + VEH (n = 7), WT + HDM (n = 8), IL-1β KO + VEH (n = 8), and IL-1β KO + HDM (n = 10). n.s: not significant, * $P < 0.05$, ** $P < 0.01$, *** $P < 0.001$, **** $P < 0.0001$ (one-way ANOVA with post hoc Bonferroni's test). Figure 3 is currently being prepared for submission for publication of the material. Wang, Dong-Jie; Chang, Han; Bertin, Samuel. "Chronic Exposure to House Dust Mites Accelerates Lung Cancer Progression in Mice by Activating the NLRP3/IL-1β Pathway in Lung Macrophages." The thesis author is a co-author of the materials.

Single-cell RNA-Seq reveals the complexity of the murine lung microenvironment at steady-state and during chronic lung inflammation

Based on the data presented above, we hypothesize that chronic HDM exposure induces persistent IL-1β production in the lung, which changes the lung microenvironment and makes it conducive to tumor growth. To test the hypothesis, we performed scRNA-seq and analyzed the effects of HDM exposure and IL-1β signaling on the various cell types present in the lungs. We treated WT and IL-1β KO mice with VEH or HDM for 5 weeks (Fig. 6A), harvested and sorted live cells by FACS, and loaded approximately 16,500 cells per sample in duplicate on the 10X Genomics Chromium Platform (Fig. 6B, C).

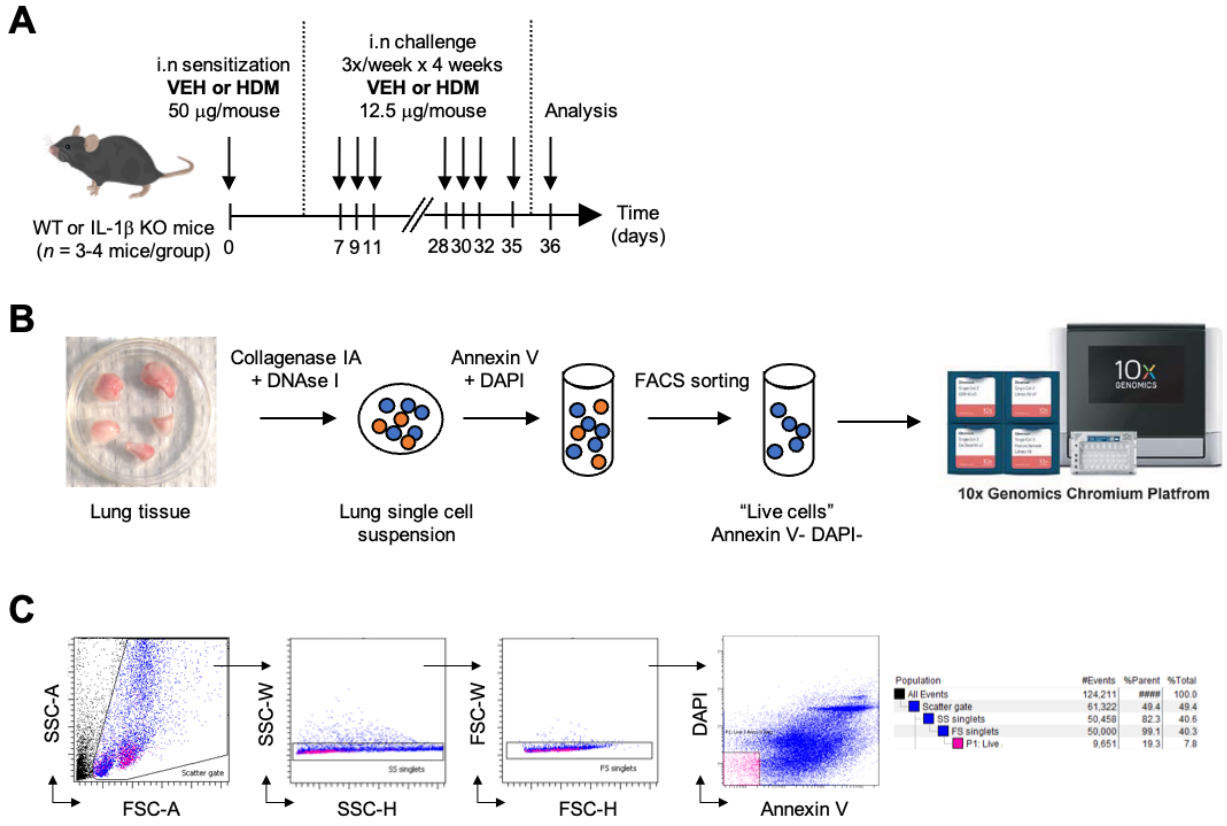

Figure 4. Schematic overview of the scRNA-seq experiment. **A)** Age- and sex-matched WT and IL-1β KO C57BL/6 mice were treated i.n with VEH or HDM for 5 weeks as indicated in this schematic overview of the study design. **B)** Lung tissues from mice were harvested 24 hours after the last i.n treatment, enzymatically digested, and the resulting single cells were stained with Annexin V and DAPI. Live single cells were sorted by FACS and were loaded onto the Chromium Controller (10x Genomics). **C)** Representative flow cytometry plots showing FACS sorting results for Annexin V and DAPI double-negative cells (P1: Live gate). WT + VEH (n = 4), WT + HDM (n = 4), IL-1β KO + VEH (n = 3), and IL-1β KO + HDM (n = 3).

A) Single-cell metrics

We performed scRNA-seq using 10X Genomics with the FACs sorted pooled samples. A total of 62,690 cells were captured from all samples, with the mean of 218 million total reads for each sample. All samples had high-quality reads with Q30 above 90%, excellent mapping rates to the murine genome of a mean 94.9%, and an average of 1795 UMI per cell. For quality control, initial 62,690 cells with high mitochondrial gene percentage (>5%) and fewer gene counts (<500) were filtered to remove outliers such as dying cells, doublets, or multiplets, which yielded a total of 49,699 cells for downstream analysis. The quality control metrics for the scRNA-seq data from all samples are summarized in Table 1.

Table 1. Single-cell metrics. WT mice treated with vehicle (WT_VEH) or HDM (WT_HDM) and IL-1β mice treated with vehicle (KO_VEH) or HDM (KO_HDM) were loaded in duplicates (as presented in the column of Samples) on 10X Genomics Chromium Controller using the Single Cell 3' kit v3.1 Dual Index for barcoding, GEM, and library construction. After sequencing Illumina NovaSeq 6000 S4, CellRanger 5.0.1 was used to demultiplex and align the reads to the murine reference genome. The results for each sample were presented for the total reads, total cells, and fraction reads, reads per cell (Reads/cell), and genes per cell (Genes/cell), unique molecular identifier (UMI) per cell, and total genes. Seurat V3.0 was used to filter doublets or outliers based on the mitochondrial gene percentage and fewer gene counts as presented in filtered cells column.

Condition	Samples	Total Reads	Total Cells	Fraction Reads	Reads/cell	Genes/cell	UMI/Cell	Total genes	Filtered Cells
WT_VEH	A1	188M	6,840	94.8%	27,499	666	1,351	18,474	5,351
	A2	199M	6,798	95.8%	29,294	834	1,860	18,930	4,734
WT_HDM	B1	186M	7,251	95.0%	25,689	773	1,624	18,341	6,399
	B2	193M	7,408	95.2%	26,037	757	1,612	18,281	6,286
KO_VEH	C1	261M	6,816	94.7%	38,394	706	1,515	18,294	5,776
	C2	202M	7,665	95.0%	26,304	861	2,008	18,793	5,623
KO_HDM	D1	238M	11,603	94.5%	20,553	866	2,063	18,920	8,955
	D2	280M	8,309	94.0%	33,739	978	2,326	18,865	6,575

B) UMAP initial clustering results

The datasets from WT mice treated with vehicle (WT_VEH) or HDM (WT_HDM) and IL-1β mice treated with vehicle (KO_VEH) or HDM (KO_HDM) were integrated to find the cluster markers and identify cell types across the four conditions. The unbiased uniform manifold approximation and projection (UMAP) for dimensional reduction by the R package Seurat V3

initially generated 22 cell clusters [42]. The cell type prediction for each cluster was conducted by SingleR package based on Mouse RNA seq and Immgen databases and then adjusted by the known cell type markers and its differentially expressed genes (DEGs) for better prediction [43]. The clusters representing the same cell type were pooled together, generating 11 different cell clusters as follow: B cells, T cells, natural killer cells (NK), natural killer T cells (NKT), monocytes, neutrophils, endothelial cells, macrophages, fibroblast, basophils, and dendritic cells (DC) (Fig. 5A, B, Table 2). The major cell populations in our dataset were B cells, T cells, NK cells, and NKT cells (Fig. 5C). We conducted a permutation test to assess whether the population proportion of each cell type was significantly modulated between the conditions. The top differential gene expression showed that some clusters expressed distinct genes that may serve as cell type markers. The top expressed genes for B cells, basophils, endothelial cells, fibroblasts, and neutrophils were highly conserved in each cluster and specific to the cell type (Fig. 5D). However, the top differential genes were co-expressed in clusters with similar cell identities as in the group of monocytes, macrophages, and DC, and of NK, NKT, and T cells, and cell-type gene markers were less specific to each cluster, indicating that mixed cell types could be present within the clusters (Fig. 5D, E).

Table 2. Initial clustering results for 11 major cell types. The initially identified clusters are listed in the table with the number of cells from all conditions (WT_VEH, WT_HDM, KO_VEH, and KO_HDM). Each cluster highly expressed the gene markers that are known to represent the cell-type as listed.

Cluster	WT_VEH	WT_HDM	KO_VEH	KO_HDM	Gene markers
B cells	3524	4472	4038	8229	*Cd74, Igkc, Cd79a*
T cells	3461	5280	4482	5420	*Trbc2, Il7r*
NK	783	948	579	624	*Gzma, Klre1*
NKT	434	639	707	761	*Ccl5, Nkg7*
Monocytes	538	275	625	242	*Csf1r, Lyz2*
Neutrophils	389	768	223	45	*S100a9, S100a8*
Endothelial cells	615	67	427	24	*Calcrl, Ptprb, Epas1*
Macrophages	170	160	148	145	*Mpeg1, Lyz2*
Fibroblasts	132	5	147	1	*Sparc, Col3a1*
Basophils	29	57	17	39	*Mcpt8, Cd63*
Dendritic cells	10	14	6	0	*Fabp5, Cxcl16*

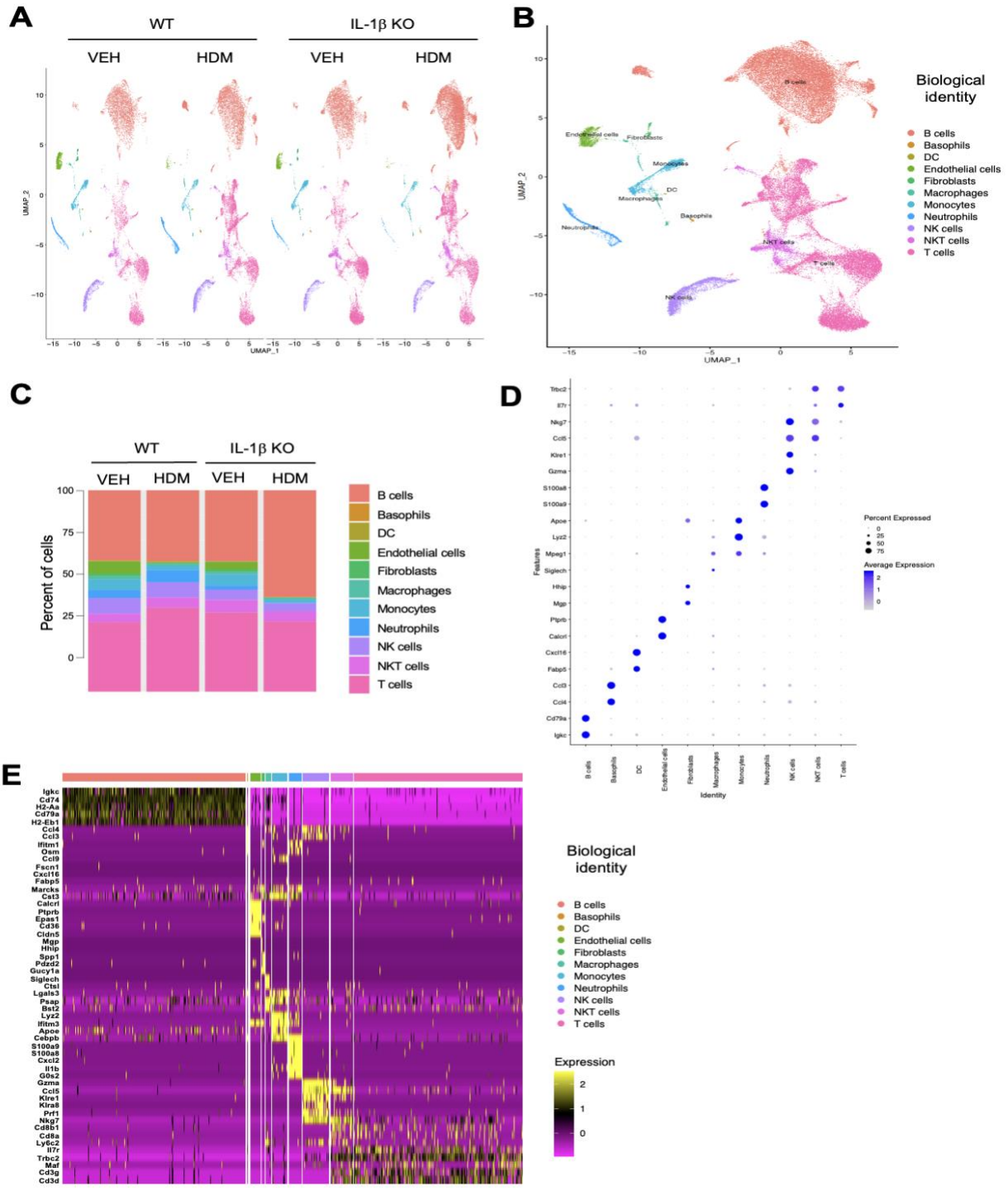

Figure 5. scRNA-seq revealed the presence of 11 major cell types in the lungs. A) UMAP representation of the 11 clusters by gene expression in WT or IL-1β mice treated with VEH or HDM**. B)** UMAP representation of the 11 clusters assignment from the pooled samples. **C)** The proportion of each cluster in the 4 different conditions. **D)** Dot plot representation of the marker genes for each cluster. **E)** Heatmap illustrating top 5 most DEGs for each cluster.

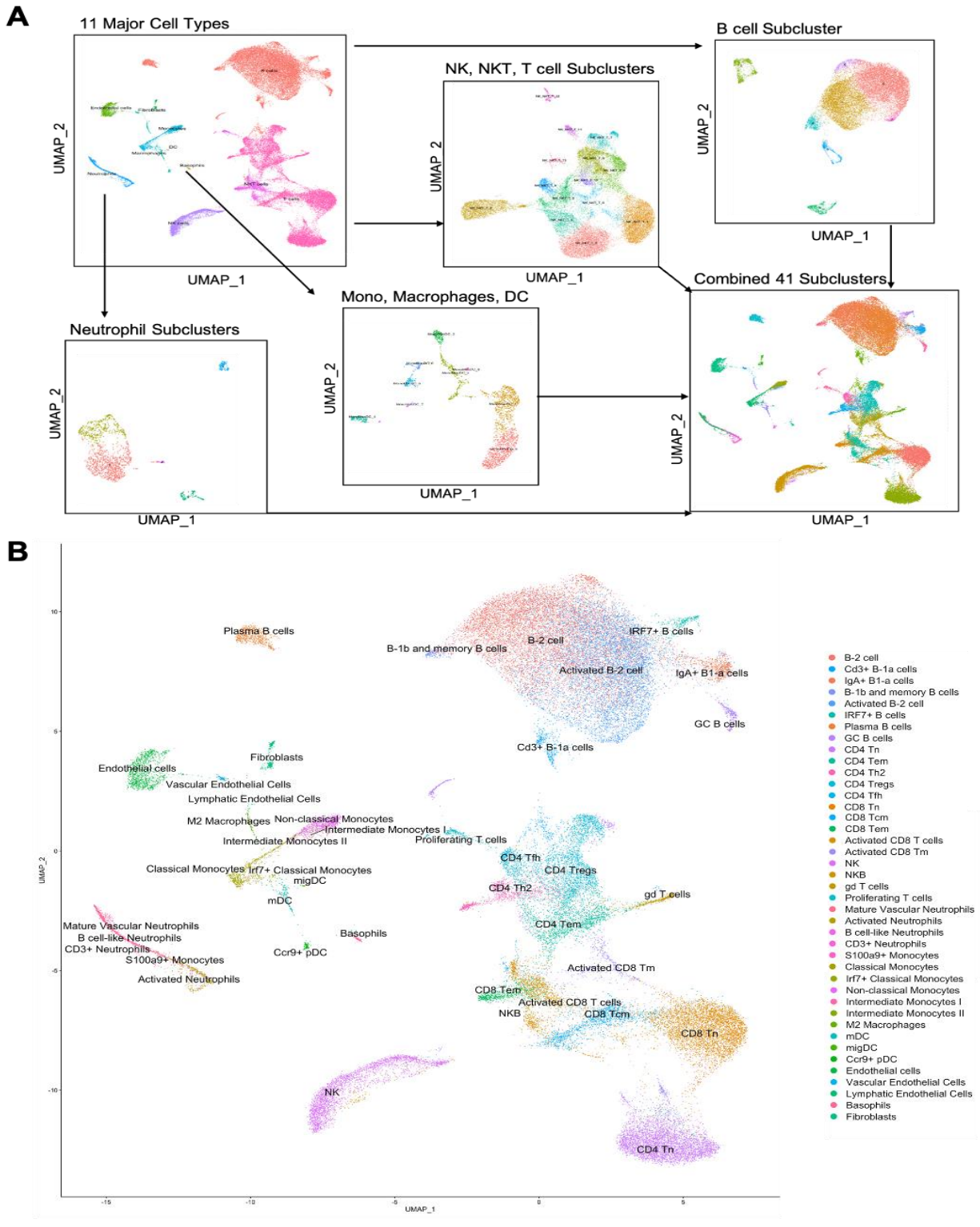

Figure 6. Subclustering of the initial 11 clusters generated 41 subclusters. A) B cells, neutrophils, the clusters of NK, NKT, and T cell, and of monocytes, macrophages, and DC were subclustered, yielding 8 B cell subclusters, 14 NK/T subclusters, 11 monocytes (mono), macrophages, DC subclusters, and 5 neutrophil subclusters. **B)** UMAP representation of combined 41 clusters in the pooled data from the four different experimental groups.

C) Subclustering results

To improve the depth and accuracy of analysis, we merged and re-subclustered the sets of monocytes, macrophages, and DC, and of T, NK, and NKT clusters with similar identities and gene expression (Fig. 6A). We also further subclustered B cells and neutrophils with adequate cell numbers (Fig. 6A) for better resolution of cell subsets. After subclustering, we yielded a total 41 clusters with distinct cell subtypes retaining distinct gene profiles with biological functions, revealing the heterogeneity and plasticity of B cells, T cells, neutrophils, monocytes, macrophages, and DC (Fig. 6B). The cell type predictions were validated by known cell type markers and the previous studies with identical gene profiles, confirming the lung cell heterogeneity based on the transcriptomic profiles. In order to focus on the specific modulations of the lung microenvironment induced by HDM exposure and IL-1β signaling, only the significantly altered lung cell subpopulations across the conditions will be discussed in this thesis.

Chronic HDM exposure and IL-1β signaling change NK and T cell development and their gene expression profiles in the lungs

A) Cell type Identification of NK and T cells

Initially labeled T, NK, and NKT clusters were merged and subclustered into 14 unique subpopulations based on UMAP (Fig. 7A). Based on the SingleR and adjusted predictions by the known gene markers for each cell type and their gene profiles concurring with the previous studies, we identified 14 different subsets of T and NK cells as follows: CD4 and CD8 naïve T cells (Tn), CD4 regulatory T cells (Tregs), CD4 effector memory T cells (Tem), CD4 follicular helper T cells (Tfh), γδ T cells, activated CD8 T cells, activated CD8 memory T cells, CD8 central memory T cells (Tcm), CD8 effector memory T cells (Tem), natural killer cells (NK), natural killer B cells

(NKB), and proliferating T cells (Table 3). The gene signatures for each cell type were highly expressed in the cluster, supporting their cell-type identity. As expected, the compositions of NK and T cell clusters were significantly different for each condition. In the VEH-treated mice, naïve CD4 and CD8 T cells were the most abundant cells, while the HDM-treated mice showed more differentiated CD4 and CD8 T cells subtypes (Fig 7B, C). The top five differential gene expressions were very distinct in each subcluster and the gene expressions were highly related to the functions and characteristics of each cell subtype (Fig. 7D). Noticeably, the initially predicted NKT cluster was subclustered into cytotoxic effector memory CD8 T cells and activated CD8 T cells, suggesting that subclustering method can reveal the better resolution of cell subsets.

Table 3. The summary of subclustering results of NK, NKT, and T cells. The cell number of each subcluster are presented in the following conditions (WT_VEH, WT_HDM, KO_HDM). SingleR prediction was first used to predict the cell type for each subcluster. We then adjusted the cell-type prediction for each cluster by using the known cell type markers that are expressed each cell type based on the previous studies.

Subcluster	WT_ VEH	WT_ HDM	KO_ VEH	KO_ HDM	SingleR Prediction	Adjusted Prediction	Cell markers
NK_NKT_T_0	1043	974	1636	1123	T cells (T.CD8.CTR)	CD8 Tn (naïve)	*Cd8a/b1, Ccr7, Sell*
NK_NKT_T_1	1166	1020	1662	921	T cells (T.CD4TESTCJ)	CD4 Tn (naïve)	*Cd4, Ccr7, Sell*
NK_NKT_T_2	769	934	559	583	T cells (T.4MEM44H62L)	NK	*Klre1, Tbx21*
NK_NKT_T_3	122	1118	91	1043	Tgd (Tgd.mat.VG2+)	CD4 Tregs	*Cd4, Foxp3, Ctla4*
NK_NKT_T_4	504	920	366	383	NK cells (NK.49CI-)	CD4 Tem (Effector Memory)	*Cd4, Tcf7, S100a4*
NK_NKT_T_5	179	437	346	698	T cells (T.8EFF.OT1LISO)	Activated CD8 T cells	*Cd8a/b1, Cxcr3, Ccr5, Gzmk, Ifng, Eomes*
NK_NKT_T_6	359	396	242	411	NK cells (NK.DAP10-)	CD8 Tcm (Central Memory)	*Cd8a/b1, Bcl2, Bcl2l11, Eomes, Il2rb,*
NK_NKT_T_7	22	149	118	660	T cells (T.Tregs)	CD4 Th2	*Cd4, Gata3, Il1rl1, Il13, Areg, Il4*
NK_NKT_T_8	83	319	174	206	T cells (T.4MEM44H62L)	Activated CD8 Tm (memory)	*Cd8a/b1, Irf7, Stat1, Bcl2, Bcl2l11*
NK_NKT_T_9	229	116	377	33	T cells (T.8MEM.OT1.D45.LI SOVA)	CD8 Tem (effector memory)	*Cd8a/b1, Cx3cr1, Ccl5, Gzmb*
NK_NKT_T_10	16	264	9	371	T cells (T.8Mem)	CD4 Tfh (Follicular helper T)	*Cd4, Tcf7, Cxcr5, Bcl6, Il21*
NK_NKT_T_11	90	88	90	168	T cells (T.Tregs)	γδ T cells	*Trdc, Tcrg-C1, Cxcr6, Il7r, Il1r1, Rora*
NK_NKT_T_12	69	67	51	114	T cells (T.8Mem)	NKB cells	*Cd74, Cd79a, Cd79b, Gzma, Ncr1, Klrc2*

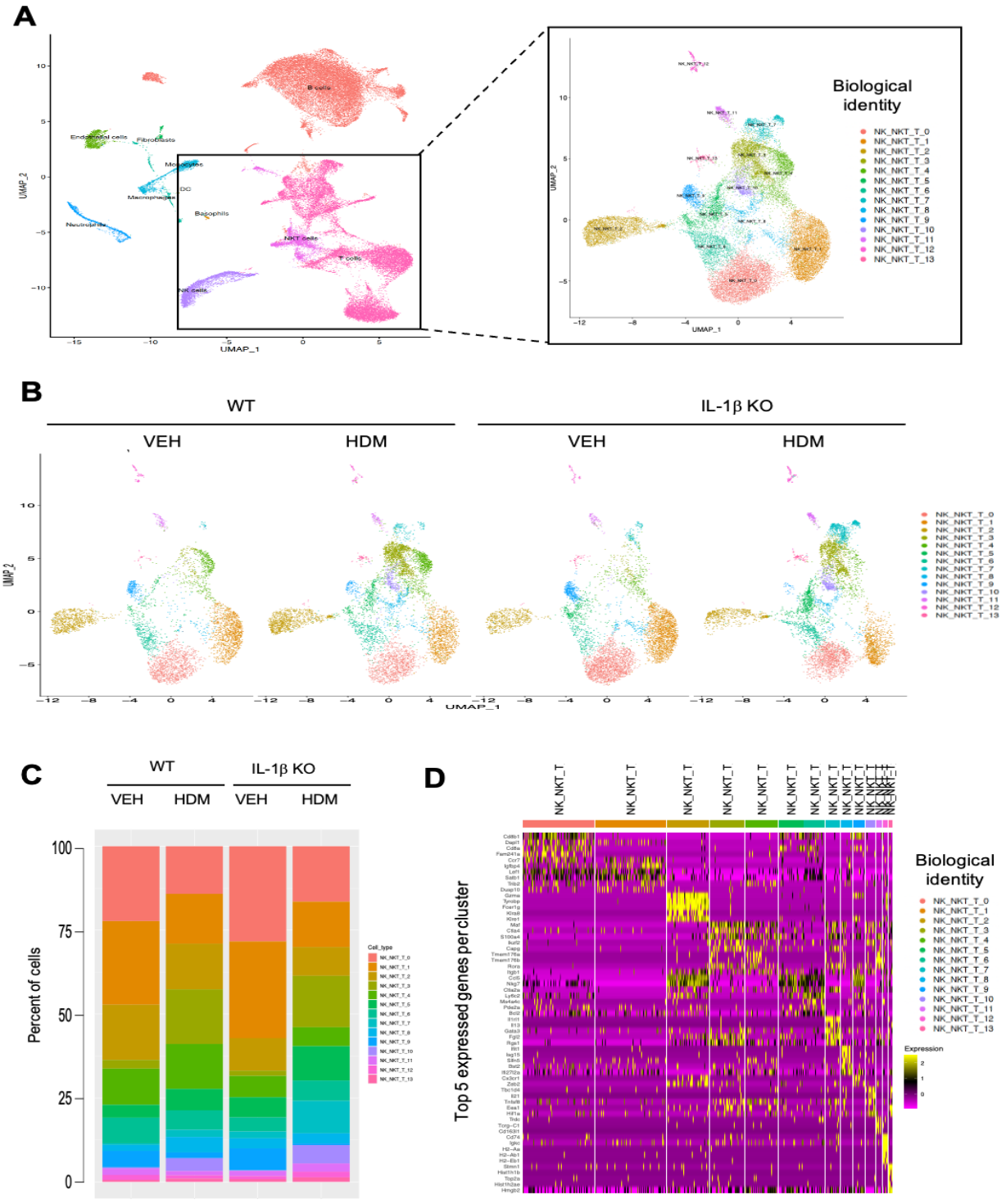

Figure 7. Single-cell profile of NK, NKT, and T cell subclusters in the murine lungs. A) Two-dimensional UMAP projection of subclustering results from initial NK, NKT, and T cell subclusters. **B)** Two-dimensional UMAP projection of NK, NKT, and T cell subclusters from four different conditions: WT mice treated with VEH or HDM, and KO mice treated with VEH or HDM. **C)** The cell population proportions of each cluster in four different conditions. **D)** Heatmap shows the top 5 upregulated DEGs of the 14 clusters, identified in UMAP plot. The value of gene expression was scaled by Log2 fold change.

A) HDM exposure upregulated CD4 Regulatory T cells in an IL-1β-independent manner but IL-1β signaling affected their differentiation.

Tregs were identified in the subcluster (NK_NKT_T_3) based on the expression of the Treg signature genes *Cd4, Foxp3,* and *Ctla4.* The top DEGs in this cluster were *Icos, Ikzf2, S100a4, S100a6, S100a11, Tnfrsf4,* and *Capg,* which were confirmed to be the top DEGs of Tregs in the previous study [44]. We observed a significant upregulation of Tregs in both WT and IL-1β KO mice upon chronic HDM exposure (122 cells in WT_VEH to 1,118 cells in WT_HDM, and 91 cells in KO_VEH to 1,043 cells in KO_HDM) (Table 3), indicating that the upregulation of Tregs in response to HDM is IL-1β-independent.

Due to the previously known heterogeneity and plasticity of Tregs in different cues [45-47], we evaluated the effect of HDM and IL-1β on Tregs phenotypes by the DEG analysis of the Treg subcluster between the conditions. As expected, Tregs in our data expressed distinct gene profiles under different conditions. In both WT and IL-1β KO mice treated with VEH, Tregs expressed a high level of tissue-resident- and naïve Treg-related genes (*Areg, Ctla2a*, *Klf2*), while in HDM-treated mice Tregs highly expressed *Maf* (encoded transcription factor is required for Treg-derived IL-10 secretion), representing mature or effector Tregs (Fig. 8A) [48-51]. Interestingly, *Il17a* was upregulated only in WT mice treated with HDM therefore indicating a role for IL-1β in the induction of IL-17-expressing Tregs.

B) HDM exposure downregulated CD8 effector memory T cells in an IL-1β-independent manner

$CD8^+$ effector memory T cell (Tem) was identified in the subcluster (NK_NKT_T_9) based on the signature gene marker *Cx3cr1*, *CD8a1*, and *CD8b2*, as well as cytotoxicity related

genes, *Gzma, Gzmk, Gzmb, and Klrc1*, that are known to be expressed in $CD8^+$ Tem [52]. The top DEGs corresponded to the characteristics of CD8 Tem such as *Zeb2* (promote terminal differentiation of Tem), *Ccl5* and *Ccl4 (*chemokine-encoding genes), and *Ifng* (IFN-γ encoding gene) [53, 54]. The cell population of this subset was significantly downregulated by HDM in both WT (229 cells in WT_VEH to 116 cells in WT_HDM; 4.9% to 1.69%) and IL-1β KO (377 cells in KO_VEH to 33 cells in KO_HDM; 6.54% to 0.49%) mice, possibly indicating that HDM inhibits the generation of *Cx3cr1*$^+$ CD8 Tem. DEGs between conditions revealed that *S100a4* was the only gene significantly upregulated by HDM in KO mice, but the encoded protein S100A4 expressed in Tem was known to be rather dispensable for Tem cell development [55].

C) HDM exposure upregulated CD4 Th2 cells particularly in absence of IL-1β

Th2 $CD4^+$ cells (NK_NKT_T_7 subcluster) were identified by the expression of the signature markers *Il1rl1, Il13, Gata3, Areg,* and *Il4*. The DEGs in this cluster included *Il2ra, Il5, Il9r, Il13, Cxcr6, Il10, Tgfb1, and Ctla4*, which are all known to be expressed in $CD4^+$ Th2 cells. While HDM treatment upregulated Th2 $CD4^+$ cells in both WT (22 cells in WT_VEH to 149 cells in WT_HDM) and IL-1β KO mice (118 cells in KO_VEH to 660 cells in KO_HDM) (Table 3), $CD4^+$ Th2 cells were significantly more numerous in KO than in WT mice treated with HDM (Fig. 7B, C). The subpopulation differences between conditions indicated that chronic HDM exposure elicited Th2 response in murine lungs, but interestingly, more so in absence of IL-1β. The phenotype of $CD4^+$ Th2 was not altered by IL-1β as the DEG analysis between the conditions showed no modulation between WT_HDM and KO_HDM. This finding suggests an inhibitory role of IL-1β signaling on Th2 cell differentiation in the lungs.

D) HDM exposure upregulated CD4 Effector Memory T cells in an IL-1β-dependent manner

CD4+ effector memory T cells (NK_NKT_T_4 subcluster) were identified by the known cell-type markers based on the gene expression (*Cd3*$^{+}$, *Cd4*$^{+}$, *Tcf7*$^{+}$, *Ccr7*$^{-}$, *Sell*$^{-}$, *CD28*$^{+}$). The top DEGs included *S100a4* (preferentially expressed in effector memory T cells) [55], *Tmem176a* and *Tmem176b* (expressed in Th17 cells) [56, 57], *Rora* (expressed in activated CD4+ T cells) [58], *Itgb1* (most expressed in terminal effector memory T cells), and *Lsp1* (induced by T cell activation) [59]. The DEG analysis found that there was a significant downregulation of Th17-associated genes (e.g., *Tmem176b*) in IL-1β KO mice [58, 60, 61], indicating the role of IL-1β during Th17 polarization (Fig. 8B). The upregulation of CD4^{+} Tem in WT mice treated with HDM and the DEGs between the conditions suggest that T cells were preferentially polarized toward Th17 upon chronic HDM exposure in presence of IL-1β.

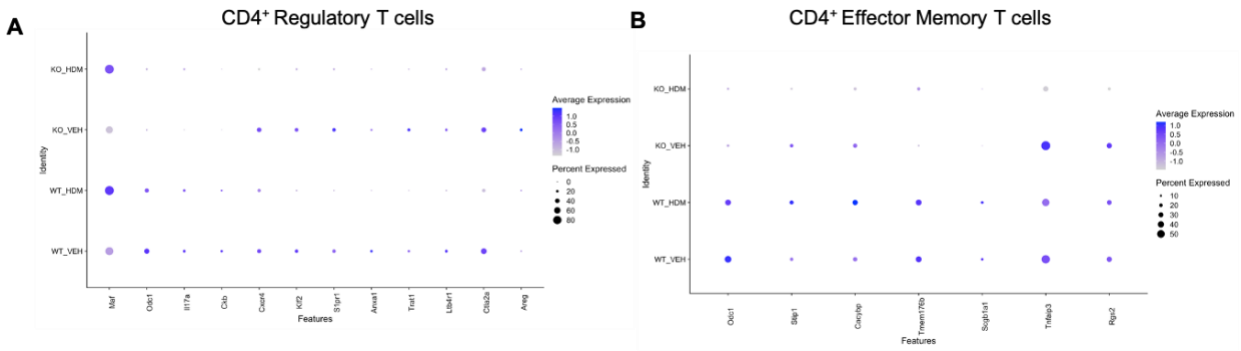

Figure 8. DEG analysis for CD4+ regulatory T cells and effector memory T cells. A) The genes (*Maf, Odc1, Il17a, Ckb, Cxcr4, Klf2, S1pr1, Anxa1, Trat1, Ltb4r1, Ctla2a, Areg*) that were differentially expressed in the following conditions (WT_VEH, WT_HDM, KO_HDM) are presented in a dot plot. **B)** The DEGs (*Odc1, Stip1, Cacybp, Tmem176b, Scgb1a1, Tnfaip3, Rgs2*) between WT_HDM and KO_HDM in CD4^{+} effector memory T cells are shown in a dotplot. Average expression is presented by the log2 fold change of gene expression. Predicted genes and heat shock protein-encoding genes were omitted in the analysis. The significance was determined by the adjusted p-value (<0.05) based on Bonferroni correction and average log2 fold change (>0.75).

Chronic HDM exposure and IL-1β signaling induced B cell development and differentiation.

A) B cell subtypes

The largest number of cells (20263 cells; 40.77% of all cells in the pooled samples) (Table 2) were identified as B cells as they exclusively expressed B cell antigen receptor genes (*Cd79a, Cd79b)*, and MHC II encoding genes (*Cd74, H2-Aa, H2-Eb1*) (Fig. 5D, E). For a better resolution of cell subset identities, the B cell cluster was subclustered into 8 subclusters (Fig. 9A), which revealed both known and unique B cell subtypes based on the cell type markers and previous studies on B cell gene profiles (Table 4). In both WT and KO mice, chronic HDM exposure significantly upregulated activated B-2 cells, plasma B cells (*Igha*$^+$ or *Ighg1*$^+$), IgA secreting B1-a cells, germinal center (GC) B cells, and *Irf7*+ B cells (Fig. 9B, C and Table 4), which indicated the activation of humoral immunity by chronic HDM exposure.

Table 4. B cell Subclustering Results Summary. The cell number of each B subcluster are presented in the following conditions (WT_VEH, WT_HDM, KO_HDM). SingleR prediction was first used to predict the cell type for each subcluster. We then adjusted the cell-type prediction for each cluster by using the known cell type markers and compared the gene profiles of each cell type with the previous studies as presented in Cell markers.

Subcluster	WT_VEH	WT_HDM	KO_VEH	KO_HDM	SingleR Prediction	Adjusted Prediction	Cell Type Markers
B_cell_0	3041	2061	3383	1330	B cells (B.Fo)	B-2 cell	*Ighm, Ighd, Ebf1, Foxp1*
B_cell_1	126	1378	164	5200	B cells (B.Fo)	Activated B-2 cell	*Samsn1, Ifi30, Dock10, Il4i1*
B_cell_2	175	163	174	555	T cells (T.8Mem)	Cd3+ B-1a cells	*Cd3d/e/g, Fyb, Trac, Cd5*
B_cell_3	46	357	53	209	B cells (B1a)	Plasma B cells	*Jchain, Xbp1, Irf4, Igha, Ighg1*
B_cell_4	34	198	34	390	B cells (B.CD19CONTROL)	IgA+ B1-a cells	*Igha, Cd86, Cd44*
B_cell_5	12	156	5	303	B cells (B.GC)	GC B cells	*Bcl6, Rgs13, Basp1*
B_cell_6	64	132	97	152	B cells (B.Fo)	Irf7+ B cells	*Irf7, Ifit3, Stat1*
B_cell_7	26	27	128	90	B cells (B1b)	B-1b and memory B cells	*S100a6, Zbtb2*

B) HDM exposure upregulated activated B-2 cells, particularly in absence of IL-1β

B-2 cells (B_cell_0 subcluster), also known as follicular B cells, were the most abundant cell subtype in our data (9,660 cells; 47.67% of all B cells), identified by the co-expression *Ighm* and *Ighd* (IgM and IgD heavy chain encoding genes) as well as *Ebf1* (B cell maintenance transcription factor encoding gene), and *Foxp1* (Mature B cell survival regulating transcription factor encoding gene) (Fig. 9D and Table 4) [62].

The activated B-2 cells (B_cell_1; 6930 cells; 34.2% of the B cells) expressed the identical genes as B-2 cells (*Ebf1, Foxp1, Ighm,* and *Ighd*), but differentially expressed IL-4- or LPS-inducible genes such as *Il4i1* (IL-4-induced gene-1), *Samsn1* (upregulated in activated B cell by IL-4 or LPS) [63] *Ifi30* (Gamma-Interferon-Inducible Protein-coding gene in response to LPS), *Dock10* (induced by IL-4 in B cell and involved in B cell development and function) [64], and Ccr6 (upregulated on B cells after activation) [65] (Fig. 9D and Table 4). HDM treatment upregulated this subset in WT (128 cells in WT_VEH to 1,395 cells in WT_HDM), but more so in IL-1β KO (175 cells in KO_VEH to 5,232 cells in KO_HDM) (Table 4). The DEG analysis revealed that there was no major differences between WT_VEH and KO_VEH, whereas 50 genes and 68 genes were differentially expressed between WT_HDM and KO_HDM and between KO_VEH and KO_HDM, respectively (data not shown). Among them, IL-4 induced genes (*Il4i1*, *Ifi30*, *Samsn1*, and *Dock10*) were expressed at a higher level in HDM-treated IL-1β KO mice (Fig. 10). Based on the gene profiles of activated B-2 cells with IL-4-inducible genes, the significant upregulation of activated B cells in KO_HDM may be due to the Th2-biased immune response induced by chronic HDM exposure in absence of IL-1β.

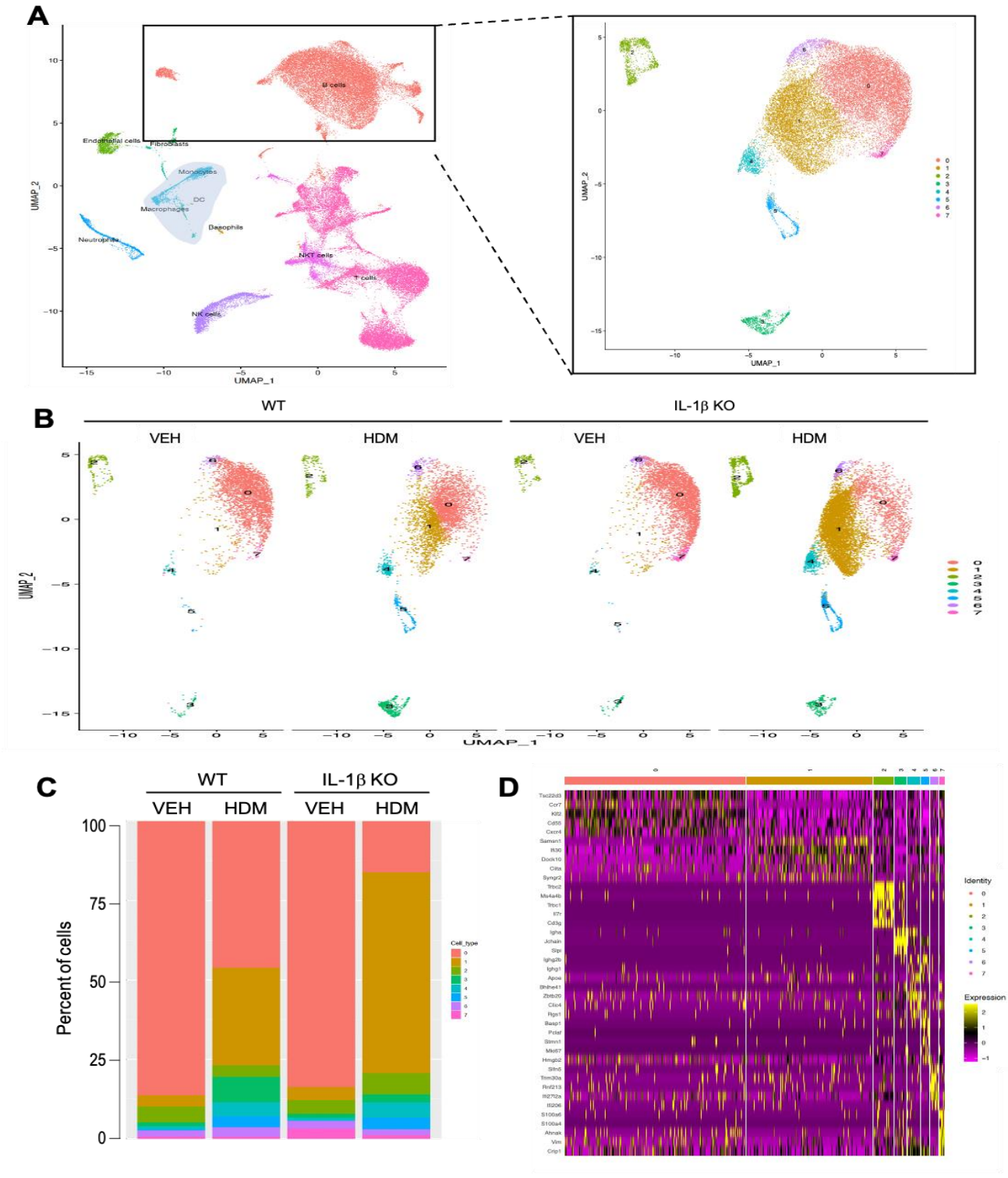

Figure 9. Single-cell profile of B cell subclusters in the murine lungs. A) Two-dimensional UMAP presentation of eight B cell subclusters from the initial B clusters by resolution of 0.2. **B)** Two-dimensional UMAP presentation for WT_VEH, WT_HDM, KO_VEH. **C)** Bar graph showing cell population proportion across four conditions in ratio. D) Heatmap of the top five DEGs in the eight subclusters. The value of gene expression was scaled by Log2 fold change.

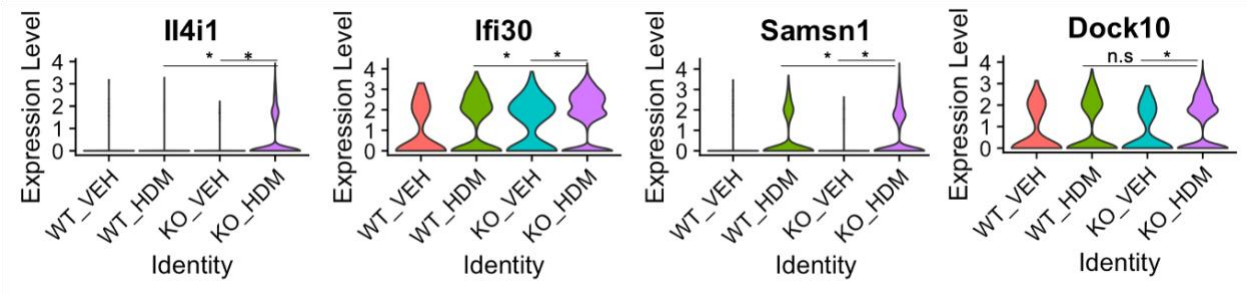

Figure 10. The differential gene expression in the activated B cells. Violin plot show that *Il4i1*, *Ifi30*, *Samsn1*, and *Dock10* genes were more upregulated in KO mice treated with HDM compared to WT mice treated with HDM or KO mice treated with VEH. The significance was determined by the adjusted p-value (<0.05) based on Bonferroni correction.

Chronic HDM exposure induced distinct monocyte, macrophage, and DC development and differentiation

A) Monocyte, macrophage, and DC subsets

We merged initial clusters of monocytes, macrophages, and DC altogether and then subclustered them into ten distinct subsets for a better resolution of cell identities (Fig. 11A). As the subclustering results provided clearer gene profiles, we identified four monocyte subsets (classical, non-classical, and two intermediate monocytes subsets), three DC subsets (plasmacytoid DC [pDC], migratory DC [migDC], and monocyte-derived DC [moDC]), M2 macrophages, and unexpectedly vascular and lymphatic endothelial cells within the cluster (Table 5). As expected, the compositions of monocytes, macrophages, and dendritic cell subsets were significantly different for each condition (Fig. 11B, C).

B) Chronic HDM exposure induced M2 macrophage differentiation via the IL-1β signaling pathway

M2 macrophages were identified by the known M2 markers *Chil3* (the gene encoding the Ym-1 protein), *Arg1*, and *Mrc1*. The top DEGs included *Mmp12* (the gene encoding a matrix

metalloproteinase involved in tissue remodeling and wound repair), *Spp1* (SPP1 protein is highly expressed in lung adenocarcinoma and a poor prognostic marker) [66], and *Il1rn* (encodes an IL-1 receptor antagonist which inhibits IL-1α and IL-1β binding) (Fig. 11D). This subcluster also significantly upregulated the expression of chemokine encoding genes such as, *Ccl6* (chemoattractant for macrophage), *Cxcl2* (chemoattractant for neutrophils), *Ccl24* (chemoattractant for basophils, eosinophils, and Th2 cells) [67], and *Ccl9* (chemoattractant for DC and myeloid-derived suppressor cells) [68]. Lastly, it upregulated *Slpi* (secreted leukocyte protease inhibitor) which may protect epithelial tissues from serine proteases and can elicit an anti-inflammatory response by inhibiting inflammasome-mediated IL-1β maturation [69].

HDM treatment significantly increased the M2 macrophage population in WT mice, but not in IL-1β KO mice, suggesting an IL-1β-dependent induction of M2 macrophages (Fig. 11B, C). Based on the gene expression related to tissue repair and resolution of inflammation such as *Mmp12* (associated with tissue remodeling, wound repair, and progression of tumor invasion), *Ilr1rn* (encoded antagonist blocks IL-1 cytokine binding), *Slpi* (inhibits inflammasome-mediated IL-1β maturation as mentioned above), this subset may play a role in mediating the resolution of tissue damage and IL-1β-mediated inflammation in the lungs [70]. In addition, M2 macrophages may also contribute to the formation of an immunosuppressive lung microenvironment and support lung cancer development [71].

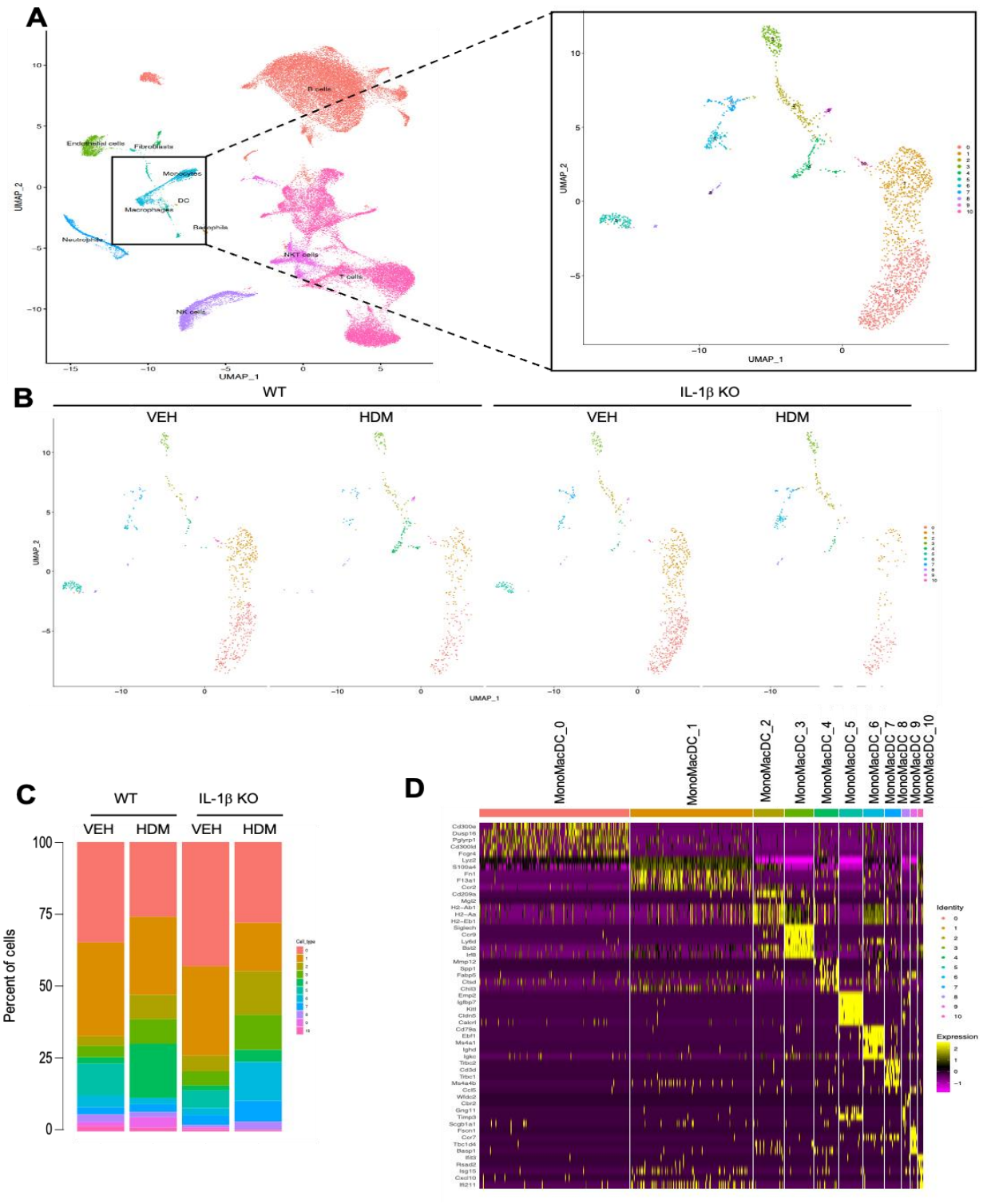

Figure 11. Single-cell profile of monocytes, macrophages, and DC subclusters in the murine lungs. A) Two-dimensional UMAP presentation of ten subclusters from the merged monocyte, macrophages, and DC clusters. **B)** Two-dimensional UMAP presentation of subclusters for WT_VEH, WT_HDM, KO_VEH, and KO_HDM. **C)** Bar graph showing cell population proportion represented by ratio across the four conditions. **D)** Heatmap of the top five DEGs in the eight subclusters. The value of gene expression was scaled by Log2 fold change.

Table 5. Re-clustering and cell type prediction of monocytes, macrophage, and DC subsets. The cell number of monocyte, macrophage, and dendritic subclusters are presented in the following conditions (WT_VEH, WT_HDM, KO_HDM). SingleR prediction was used to predict the cell type for each subcluster. Cell-type prediction was adjusted based on the known cell type markers from the previous studies as presented in Cell markers.

Subcluster	WT_ VEH	WT_ HDM	KO_ VEH	KO_ HDM	SingleR Prediction	Adjusted Prediction	Gene Markers
MonoMacDC_0	249	116	334	108	Monocytes (MO.6C-IIINT)	Non-classical Monocytes	*Csf1r, Cx3cr1, Fcgr4, Adgre4*
MonoMacDC_1	233	121	241	65	Monocytes (MO)	Classical Monocytes	*Ccr2, Ly6c2*
MonoMacDC_2	23	38	42	58	DC (DC.103-11B+F4-80LO.KD)	moDC	*Cd209a, Ccr2, Itgax*
MonoMacDC_3	29	38	39	47	DC (DC.PDC.8-)	Ccr9+ pDC	*Siglech, Ccr9, Spn,*
MonoMacDC_4	16	84	13	16	Macrophages (MFIO5.II+480INT)	M2 Macrophage	*Chil3, Arg1, Mrc1, Mpeg1*
MonoMacDC_5	79	0	47	0	Endothelial cells (BEC)	Vascular Endothelial Cells	*Egfl7, Flt1*
MonoMacDC_6	29	10	19	52	Monocytes (MO.6C-IIINT)	Intermediate Monocytes I	*Csf1r, Ccr2 H2-Ob Cd79a*
MonoMacDC_7	18	12	27	28	Monocytes (MO.6C-IIINT)	Intermediate Monocytes II	*Csf1r, Ccr2 Cd3e, Trdc1*
MonoMacDC_8	19	8	6	11	Endothelial cells (LEC)	Lymphatic Endothelial cells	*Ccl21a, Flt4*
MonoMacDC_9	10	16	5	0	DC (DC.8-4-11B+)	migDC	*Ccr7, Fscn1, Cacnb3, Mmp25*
MonoMacDC_10	13	6	6	2	Monocytes (MO)	Irf7+ Classical Monocytes	*Irf7, Ifit3, Csf1r, Ly6c2, Ccr2*

Table 6. Reclustering and Cell Type Prediction of Neutrophil subsets. The cell number of neutrophil subclusters are presented in the following conditions (WT_VEH, WT_HDM, KO_HDM). SingleR prediction was used to predict the cell type for each subcluster. Cell-type prediction was adjusted based on the known cell type markers from the previous studies as presented in Cell markers.

Subcluster	WT_ VEH	WT_ HDM	KO_ VEH	KO_ HDM	SingleR Prediction	Adjusted Prediction	Gene markers
Neut_0	295	350	158	14	Neutrophils (GN.ARTH)	Mature Vascular Neutrophils	*Mmp8, Retnlg, Sell, Itgam, Itgal, Jaml*
Neut_1	17	344	7	7	Neutrophils (GN.ARTH)	Activated Neutrophils	*SiglecF, Cxcr4, Cd63, Ccl3, Icam1*
Neut_2	31	46	24	8	Neutrophils (GN.ARTH)	CD3+ Neutrophils	*Cd3d, Cd3e, Cd3g, Trbc2, Trbc1*
Neut_3	29	27	23	14	Neutrophils (GN.ARTH)	B cell-like Neutrophils	*Cd79a, Cd79b, H2-Ab1, H2-Eb1, Fcmr*
Neut_4	17	1	11	2	Monocytes (MO.6C-II-)	S100a9+ Monocytes	*Fcgr4, Cx3cr1, Csf1r, Apoe, Ace*

Neutrophils were upregulated by chronic HDM exposure in the lungs of WT mice but were downregulated in absence of IL-1β

Neutrophils (1425 cells; 2.86% of all cells in the pooled samples) were identified by the neutrophil-specific gene expression of *S100a8* and *S100a9* (calcium-binding proteins primarily secreted in neutrophils) (Table 2), *Cxcl2* (a major chemokine for neutrophil recruitment), and *G0s2* (cell cycle progression-associated genes in neutrophil) (Fig. 5D, E). It is worth noting that HDM treatment in WT mice significantly increased the overall population of neutrophils but reduced neutrophils in IL-1β KO mice, suggesting that IL-1β may be required for the recruitment of neutrophils under chronic HDM exposure, in line with previous studies detecting lower infiltration of neutrophils in IL-1β KO mice [72, 73]. As neutrophil was one of the most modulated cell types by HDM treatment and IL-1β signaling, further subclustering was conducted for a better resolution of bona fide neutrophil subsets [74], generating five distinct subclusters (Figure 12A and Table 6).

Subclustering revealed the plasticity of upregulated neutrophils under chronic HDM exposure in the lungs

After reclustering the initial neutrophil cluster, four subsets of neutrophils and one subset of monocytes were identified in this cluster (Fig. 12A, B). With their known gene markers and their DEG profiles, we identified mature vascular neutrophils (*Retnlg, Sell, Itgam, Itgal, Jaml,* and *Mmp8*; adhesion molecule-coding genes for neutrophil extravasation) [75, 76], activated neutrophils (*SiglecF, Cxcr4, Cd63, Ccl3,* and *Icam1*) [77], $CD3^+$ neutrophils (*Cd3d, Cd3e, Cd3g, Trbc2,* and *Trbc1*) [78], B cell-like neutrophils (*Cd79a, Cd79b, H2-Ab1, H2-Eb1,* and *Fcmr*) [79] and *S100a9*$^+$ monocytes (*Fcgr4, Cx3cr1, Csf1r, Apoe,* and *Ace*) (Fig. 12D and Table 6).

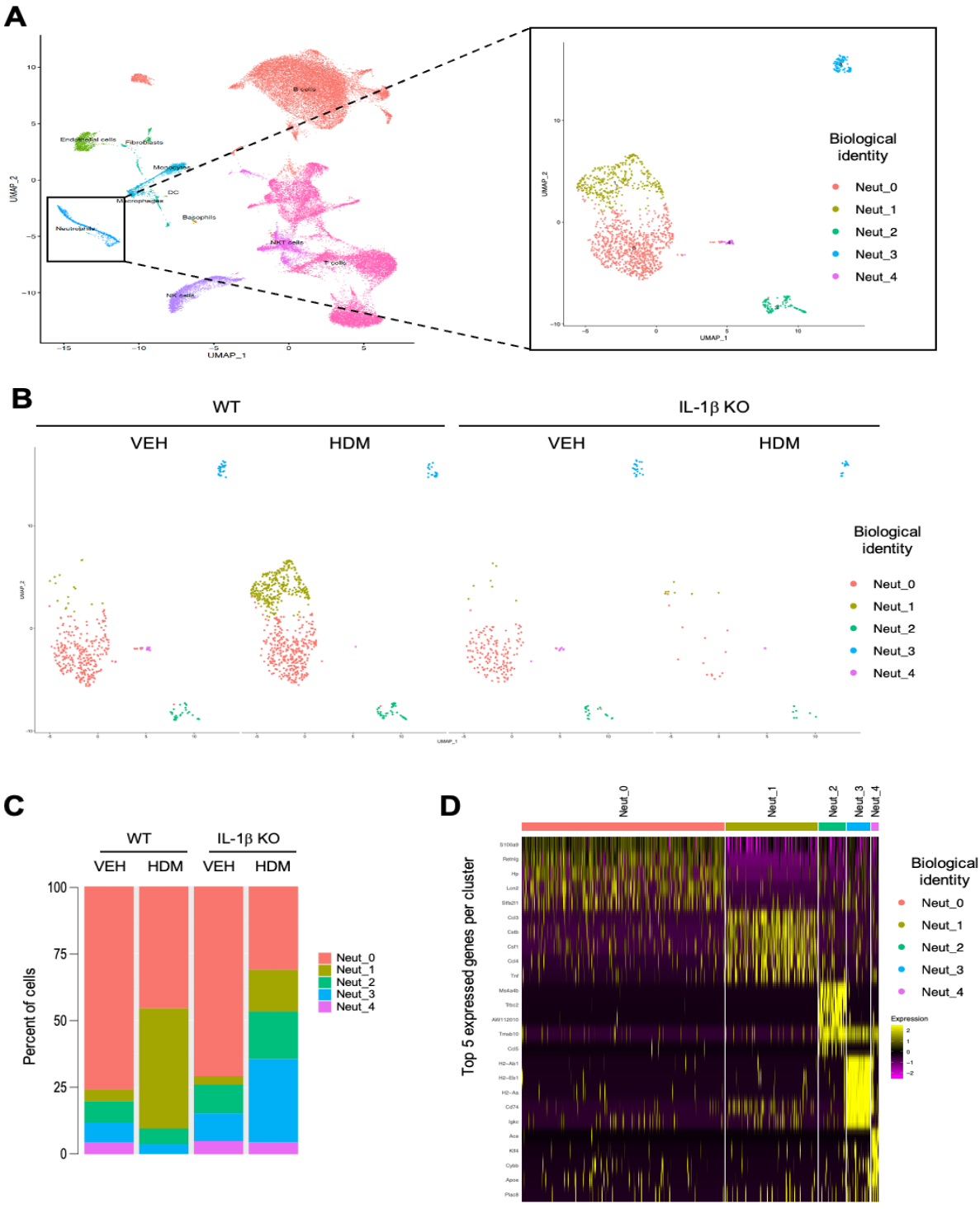

Figure 12. Single-cell profile of neutrophils in the murine lungs. A) Two-dimensional UMAP presentation of five subclusters from the neutrophil cluster by SNN resolution of 0.1. **B)** Two-dimensional UMAP presentation of subclusters for WT_VEH, WT_HDM, KO_VEH, and KO_HDM. **C)** Bar graph showing neutrophil cell population proportion represented by ratio across the four conditions. The significance of population proportion difference between the condition was calculated by permutation test. **D)** Heatmap of the top five DEGs in the five subclusters. The value of gene expression was scaled by Log2 fold change.

Activated neutrophils were exclusively found in WT mice exposed to HDM, indicating the specific recruitment of neutrophils in response to HDM in an IL-1β-dependent manner. The DEGs of activated neutrophils included chemokine, cytokine, and growth factor encoding genes (*Ccl3, Ccl4, Cxcl10, Tnf, Csf1, and Il1a*), antiapoptotic BCL-2A1 genes (*Bcl2a1a, Bcl2a1b, Bcl2a1d*), and lysosomal cysteine proteases cathepsin-encoding genes *(Ctsz, Ctsb, Ctsd, Ctss)* for lysosomal activities, as well as *Cd274* (PD-L1). Based on the gene expression, this neutrophil represented specific neutrophilic response against HDM challenge.

scRNA-seq indicated that neutrophils were the major IL-1β-expressing cell type in the lung microenvironment

Il1b was one of the top DEGs in the neutrophil cluster. Although *Il1b*, as well as *Nlrp3* gene expression, was not modulated by HDM treatment in neutrophils based on our data, HDM treatment upregulated the overall neutrophil cell population particularly in WT mice, thereby contributing to upregulation of total *Il1b* gene expression in the lungs. We further identified all cell types expressing *Il1b* and compared the gene expression between them. While all neutrophils, monocytes, and macrophages expressed *Il1b* (Fig. 13A, B), mature vascular neutrophils and activated neutrophils subset most strongly expressed *Il1b*, suggesting that these neutrophils subtypes are the major cell types producing IL-1β in the lung microenvironment.

scRNA-seq revealed different cell types expressing Ccr2

CCR2, the main CCL2 receptor, is known to be expressed in monocytes and to be involved in their recruitment to inflammatory sites [80]. As we found that blocking CCL2 inhibited the lung cancer-promoting effect of HDM (Fig. 2C), we further evaluate the expression of *Ccr2* in the lung

microenvironment in our scRNA-seq dataset. We found that *Ccr2* was expressed not only in monocytes, but also in other immune cells such as moDC, CD4 Th2, Tregs, and NK cells (Fig. 13C). As expected, the classical monocyte subtypes most strongly expressed *Ccr2* [81]; nonetheless, we found that moDC, γδ T cells, CD4 Th2, Tregs, and NK cell subtypes also expressed *Ccr2* (Fig. 13D), suggesting that neutralization of CCL2 may also inhibit the recruitment of these immune cell subtypes expressing *Ccr2*.

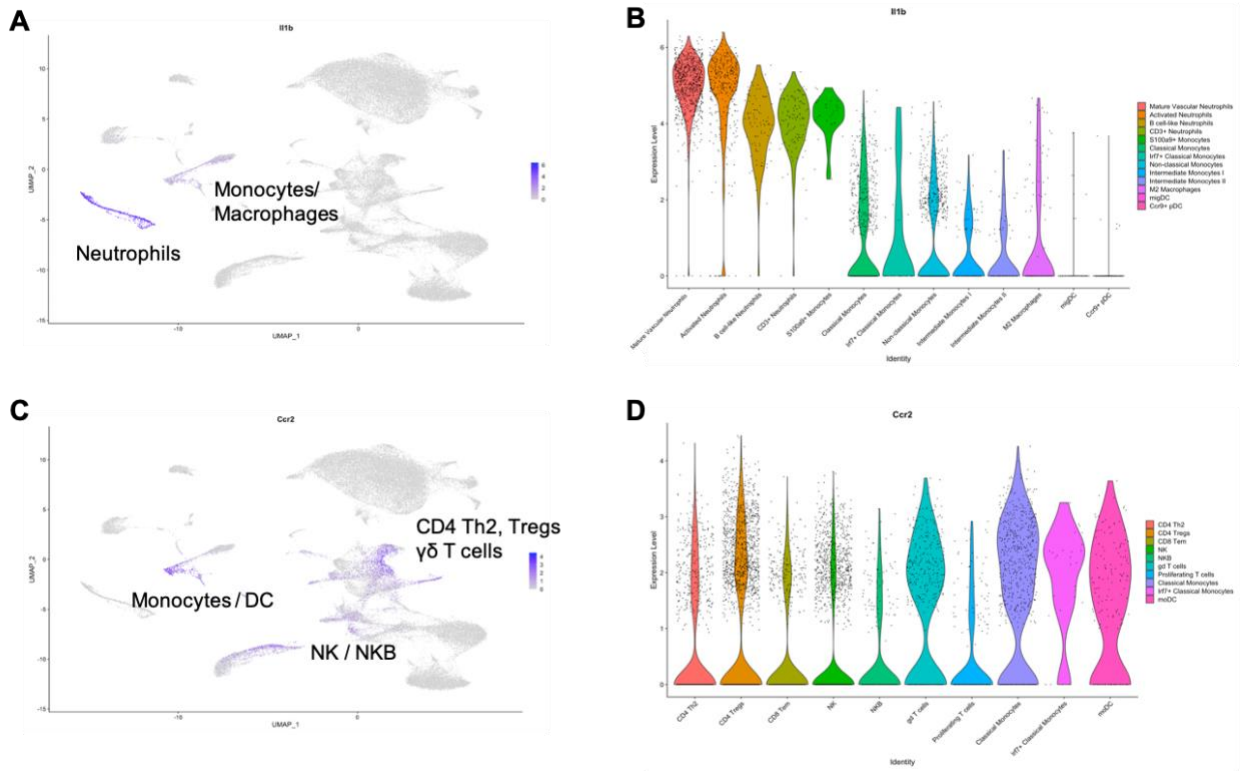

Figure 13. The scRNA-seq reveals the expression of IL-1β and CCR2 genes in each cell type. A) Neutrophils, monocytes, and macrophage clusters express *Il1b* gene as presented by two-dimensional UMAP presentation of the clusters. **B)** Violin plot shows that neutrophil subsets express the highest level of *Il1b.* **C)** Monocytes, dendritic cell (DC), CD4 Th2, Tregs, γδ T cells, natural killer (NK) and natural killer B cells (NKB) express high level of *Ccr2* as presented by two dimensional UMAP presentation of the clusters. **D)** Violin plot shows that monocyte subsets expressed highest level of *Ccr2* gene. The value of gene expression was scaled by Log2 fold change.

DISCUSSION

The association between chronic lung inflammation and lung cancer has been a significant research topic over the past decades. However, the exact mechanisms by which chronic lung inflammation promotes lung cancer are still unclear. To fill this gap of knowledge, we used chronic HDM exposure as a tool to trigger chronic lung inflammation and explored its impact on lung cancer development in mice. We first identified that chronic HDM exposure accelerated lung cancer development in two different mouse models of lung cancer, a transgenic Kras model and a carcinogen-induced model. We observed NLRP3 inflammasome activation and consequently IL-1β production in the lungs of Kras mice chronically exposed to HDM (Fig. 1). Inhibition of IL-1β by neutralizing IL-1β antibodies or IL-1β gene knockout prevented the lung tumor-promoting effect in the Kras or the urethane model, respectively (Fig. 2 and 3), suggesting that IL-1β-mediated inflammation promoted lung tumor growth. Based on these findings, we sought to further evaluate the effect of chronic HDM exposure on the murine lung microenvironment in the presence or absence of IL-1β. Due to the complexity of the lung microenvironment, previous approaches that only focused on certain cell types impose clear limitations in the analysis of the whole lung microenvironment. Here we present an extensive analysis of the cellular composition of the murine lung microenvironment at a single-cell level. To our knowledge, this is the first study assessing single-cell profiling of the murine lung microenvironment in IL-1β KO mice. We identified various cell types with distinct gene expression profiles in the murine lungs and uncovered specific effects of HDM exposure on the lung microenvironment in an IL-1β-dependent or -independent manner (Fig. 13).

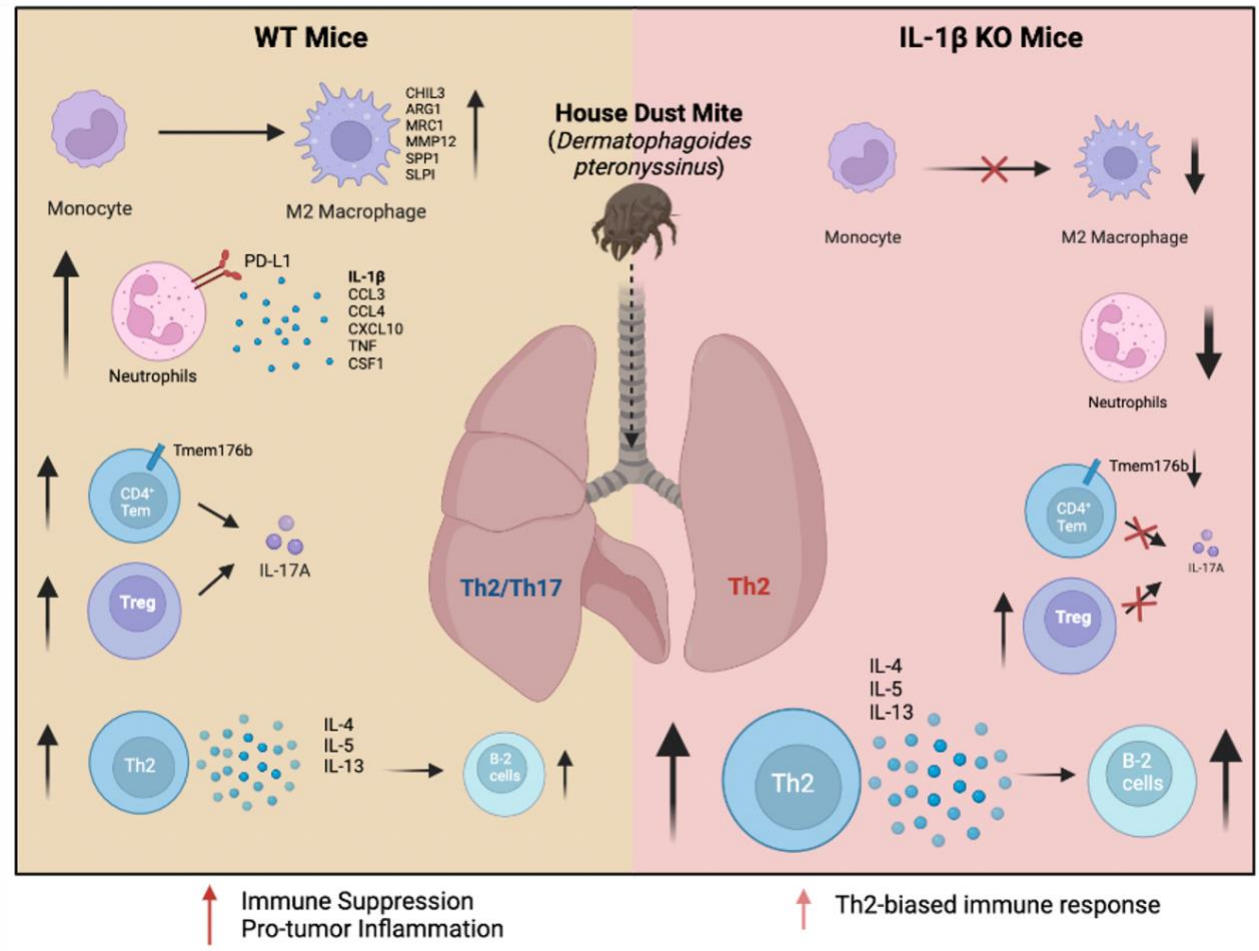

Figure 14. A summary of the impact of chronic HDM exposure on the lung microenvironment in WT and IL-1β KO mice. In WT mice, chronic HDM exposure induced a mixed Th2/Th17 inflammatory response characterized by an upregulation of M2 macrophages, IL-1β+-neutrophils, IL-17+-Tregs and -CD4+ Tem. This pro-tumor and immune-suppressive lung microenvironment induced by HDM in WT mice was not observed in IL-1β KO mice, in which chronic HDM exposure elicited a Th2-biased immune response represented by the significant upregulation of Th2 cells and activated B-2 cells producing Th2 cytokines. This schematic representation was created with BioRender.com.

First, our scRNA-seq results indicate that chronic HDM exposure induced an immunosuppressive lung microenvironment by upregulating $CD4^+$ Tregs. Tregs are widely renowned as immunosuppressive cells that can inhibit immune cell activation via CTLA-4, thereby limiting chronic inflammation and autoimmunity [82]. The upregulated $CD4^+$ Tregs may contribute to limiting DC-Thelper cell interaction [83] or inhibiting effector T cell proliferation and functions [84]. Furthermore, IL-17-secreting Tregs are known to retain immune suppression and promote an inflammatory milieu [85]. As our data suggested that IL-17-expressing Tregs were

not induced in absence of IL-1β, the induction of IL-17-expressing Tregs by HDM may support tumor growth as observed in our mouse models of lung cancer via the inhibition of anti-tumor immune responses [86]. In addition to the upregulation of $CD4^+$ Tregs, the downregulation of $CD8^+$ Tem observed in HDM-treated mice further supports this hypothesis and the induction of an immunosuppressive lung microenvironment under chronic HDM exposure. $CD8^+$ Tem are known to play an important role in immune surveillance by circulating through nonlymphoid tissues and exerting cytotoxic responses against invading pathogens [87] and during antitumor immune responses [88]. The downregulation of $CD8^+$ Tem may therefore contribute to the generation of an immunosuppressive lung microenvironment that can favor tumor development in susceptible hosts as observed in our in vivo experiments. The reductions of $CD8^+$ Tem in both WT and KO mice may be due to the upregulated Tregs [89] or direct suppression by HDM independently of IL-1β. However, the exact mechanism for the reduction in $CD8^+$ Tem needs additional research.

Next, our scRNA-seq results indicated that the polarization of the lung immune response towards Th2 or Th17 is dependent on the IL-1β signaling pathway. Indeed, we observed a mixed Th2/Th17 immune response in WT mice treated with HDM and a Th2-biased immune response in IL-1β KO mice. A previous scRNA-seq study showed a predominant Th2 response with lesser Th17 response when mice were treated with HDM for a short term on days 0, 7, and 15 [90]. Consistent with this study, we observed an upregulation of Th2 cells in WT mice, but more significantly in KO mice with chronic HDM exposure for 5 weeks. Specifically, we found that the Th2 biased immune response in KO mice was associated with a significant upregulation of CD4 Th2 cells and activated B cells with IL-4 inducible genes, and downregulation of Th17-associated genes (*Il17a, Tmem176a, Tmem176b*) within the Tregs and $CD4^+$ Tem cell populations. In contrast to the KO condition, WT mice chronically exposed to HDM not only upregulated Th17-associated

genes in both Tregs and $CD4^+$ Tem cells but also upregulated neutrophils, which are known to induce Th17 polarization in patients with severe asthma [91]. These observations indicate that IL-1β plays an important role in polarizing Th17 immune responses during chronic HDM exposure. Our data also suggest that blocking IL-1β may not be a good therapeutic target in asthma as it could exacerbate the allergic symptoms by further increasing the Th2 response.

In our mouse models, the difference between Th-biased immunity in WT and IL-1β KO mice may explain the protumorigenic effect of HDM in WT and its inhibition in IL-1β KO mice. IL-17A can promote tumor angiogenesis by upregulating vascular endothelial growth factors, thus supporting lung cancer development and progression [92-94]. Consistently, *Kras* is the most commonly mutated oncogene in non-small cell lung cancer (NSCLC), which correlated with a high level of IL-17A expression [95]. As IL-1β is known to induce alternative splicing of FOXP3, which in turn promotes Th17 differentiation [96], blocking IL-1β could inhibit Th17 cell generation and thus suppress tumor growth in NSCLC. In support of this hypothesis, IL-17A KO mice were shown to have significantly decreased NSCLC metastasis [97], and previous experiments in our lab demonstrated that tumor growth was almost completely abrogated in IL-17A KO mice in the urethane model (data not shown). Thus, blocking the IL-1β signaling pathway could be an alternative strategy to inhibit tumor growth by downregulating Th17 cells.

Among the upregulated neutrophils in WT mice treated with HDM, we identified a unique neutrophil subset displaying an aged phenotype. Neutrophils were traditionally thought to be homogenous short-lived cells, but recent studies suggest that neutrophils are heterogeneous cells, and some may live for up to 5 days [98, 99]. Consistent with previous studies, this activated neutrophil subset in HDM-treated WT mice significantly expressed neutrophil activation markers (*Sell*$^-$, *Cxcr4*^{high}), antiapoptotic genes, and most importantly *Siglecf*, which is a marker for mature,

long-lived neutrophils that can promote tumor growth [100, 101]. This subset highly expressed *Ccl3, Ccl4, Cxcl10,* and *Tnf* genes, and the encoded chemokines and the cytokine are all highly expressed in lung adenocarcinoma and may also support tumor development [102-105]. Furthermore, this subset uniquely expressed the PD-L1 encoding gene (*Cd274*), and neutrophils with PD-L1 can drive immunosuppression by suppressing $CD8^+$ T cells [106]. Based on its gene profile, this subset may therefore represent protumor neutrophils. Interestingly, this subset was almost completely inhibited in IL-1β KO mice.

Although previous experiments in the lab found that HDM activated the NLRP3/IL-1β signaling pathway mainly in lung macrophages (data not shown), we identified here that neutrophils possessed high *Il1b* and *Nlrp3* gene expression. Neutrophils are known to be a major source of IL-1β in response to different lung infections [107, 108]. Consistently, the increased number of neutrophils in WT mice exposed to HDM likely contributes to the overall upregulation of IL-1β expression in the lungs. The upregulated neutrophils expressing *Il1b* may also assist macrophages in producing IL-1β by binding IL-1 receptors or enhancing NLRP3 activation via neutrophil extracellular traps (NET) activity [109, 110]. Based on the scRNA-seq data, neutrophils may primarily contribute to IL-1β production in the early phase of the immune response (from 24 hours up to 5 days) whereas macrophages might produce IL-1β in the late phase. To evaluate the relative contribution of neutrophils vs. macrophages to the protumorigenic effect of HDM, we are currently treating $NLRP3^{Flox}S100A8^{Cre}$ (i.e., NLRP3 KO in neutrophils) and $NLRP3^{Flox}LyzM^{Cre}$ (i.e., NLRP3 KO in macrophages/myeloid cells) with HDM and with urethane. If neutrophils are found to be indispensable in promoting tumor progression in response to HDM, then neutrophils could be the main driver of lung cancer progression in our models as suggested by a recent study [111].

While monocytes and macrophages were not the major IL-1β producers in our scRNA-seq data set, we found that chronic HDM treatment may lead to differentiation of monocytes into M2 macrophages. Tumor-associated macrophages (TAMs) are another important cell type contributing to lung tumor growth and progression [112]. Macrophages can be polarized by different environmental cues into either M1 macrophages with pro-inflammatory and anti-tumor activity, or M2 macrophages leading to immunosuppression and tumor promotion [113]. Our scRNA-seq results showed that HDM changed the lung microenvironment to favor M2 macrophage induction only in presence of IL-1β. It was shown that NLRP3 could promote M2 macrophage polarization via IL-4 upregulation [114]. As Th2 immune response can lead to M2 macrophage differentiation, it was surprising to observe no upregulation of M2 macrophages in IL-1β KO mice, which have a Th2 biased immune response. Thus, the IL-1β signaling pathway may play a more important role in polarizing M2 macrophages than Th2 cells, but further research is required to validate this hypothesis. Nonetheless, the accumulation of M2 macrophages by HDM in presence of IL-1β may contribute to supporting tumor progression as evident in the Kras and the urethane models.

Together these findings suggested a connection between IL-1β-mediated inflammation and lung cancer development. The CANTOS clinical trial evaluated the effect of canakinumab (a neutralizing anti-IL-1β antibody) and found that IL-1β blockade significantly reduced lung cancer incidence and mortality, demonstrating the clinical relevance of neutralizing IL-1β in lung cancer [115, 116]. The trial's results showed that patients with the highest levels of C-reactive protein and IL-6, both downstream targets of IL-1β, trended toward earlier lung cancer diagnosis and other non-IL-1β induced cytokines did not trend with diagnosis, underscoring the importance of the IL-1β pathway in lung cancer [115, 116]. Hence, our findings are in line with clinical studies

indicating that IL-1β may be one of the drivers of lung cancer and an appropriate therapeutic target to block inflammation-induced lung cancer development.

Similar to that observed in IL-1β KO, neutralizing CCL2 also inhibited lung tumor progression in Kras mice exposed to HDM (Fig. 2B, 2C). Our scRNA-seq data suggested that CCL2 inhibition may interfere with the recruitment of mostly classical monocytes but also Tregs based to the expression of *Ccr2*. CCL2 was shown as a major chemokine recruiting Tregs and promoting M2 macrophage polarization [117, 118]. Thus, the anti-tumor effect of CCL2 neutralization our Kras model may also be due to a decreased recruitment of M2 macrophages and Treg populations.

Limitation of the scRNA-seq study

Our scRNA-seq study did not capture eosinophils and epithelial cells, as well as fibroblasts and endothelial cells. Eosinophils were similarly undetected as in other scRNA-seq study due to low RNA levels and high levels of RNase in these cells [119], which required a specific gating strategy. A previous scRNA-seq study also found the loss of endothelial cells in the diseased lung by hypoxia [120]. The loss of these cell populations in our study could also be due to our tissue dissociation protocol and/or FACS gating strategy. We might have excessively gated on the live cells (i.e., DAPI and Annexin V double negative cells) which yielded only 8% of the cells in the initial lung cell suspensions. Under these stringent sorting conditions, even the slightly damaged cells by HDM may be lost, which might explain the complete loss of fibroblasts and endothelial cells in HDM-treated mice. Epithelial cells were left out of the analysis because insufficient numbers of epithelial cells were captured potentially due to the cell sorting strategy and dead cell exclusion.

Unfortunately, we also did not capture enough myeloid cells and thus could not identify various subtypes of macrophages. As we harvested the lung tissues 24 hours after the last HDM challenge, the early responders of immunity such as B cells and neutrophils, were more likely to be collected in the samples. In contrast, peak numbers of lung eosinophils and macrophages usually occur beyond 24 hours and are usually observed 48 hours after the last HDM challenge [121, 122]. Due to the low number of myeloid cells, we could not detect any gene modulations of *Il1b* and *Nlrp3* as we originally aimed to. As both the timepoint of tissue harvest and the live cell-gating strategy introduced a bias in analyzing the cell populations in the lungs, our scRNA-seq study did not exhaustively reflect the effect of HDM exposure and IL-1β signaling on the lung microenvironment.

CONCLUSION

We have discovered that chronic HDM exposure accelerates lung cancer development in two different mouse models of lung cancer. Neutralization of either IL-1β or CCL2 inhibited the pro-tumorigenic effect of HDM in these models. Using single-cell transcriptomics, we identified various cell types within the lung microenvironment that are modulated by chronic HDM exposure and IL-1β neutralization, which may support lung cancer development. These results may help better understanding the effect of chronic lung inflammation on lung development and may have important implications for lung cancer prevention.

REFERENCES

[1] Siegel, R. L., Miller, K. D., & Jemal, A. (2020). Cancer statistics, 2020. *CA: a cancer journal for clinicians*, *70*(1), 7–30. https://doi.org/10.3322/caac.21590

[2] Sun, S., Schiller, J. H., & Gazdar, A. F. (2007). Lung cancer in never smokers--a different disease. *Nature reviews. Cancer*, 7(10), 778–790. https://doi.org/10.1038/nrc2190

[3] Conway, E. M., Pikor, L. A., Kung, S. H., Hamilton, M. J., Lam, S., Lam, W. L., & Bennewith, K. L. (2016). Macrophages, Inflammation, and Lung Cancer. *American journal of respiratory and critical care medicine*, *193*(2), 116–130. https://doi.org/10.1164/rccm.201508-1545CI

[4] Chen, L., Deng, H., Cui, H., Fang, J., Zuo, Z., Deng, J., Li, Y., Wang, X., & Zhao, L. (2017). Inflammatory responses and inflammation-associated diseases in organs. *Oncotarget*, *9*(6), 7204–7218. https://doi.org/10.18632/oncotarget.23208

[5] Chen, L., Deng, H., Cui, H., Fang, J., Zuo, Z., Deng, J., Li, Y., Wang, X., & Zhao, L. (2017). Inflammatory responses and inflammation-associated diseases in organs. *Oncotarget*, *9*(6), 7204–7218. https://doi.org/10.18632/oncotarget.23208

[6] Bousquet, J., Jeffery, P. K., Busse, W. W., Johnson, M., & Vignola, A. M. (2000). Asthma. From bronchoconstriction to airways inflammation and remodeling. *American journal of respiratory and critical care medicine*, *161*(5), 1720–1745. https://doi.org/10.1164/ajrccm.161.5.9903102

[7] Wang, D., & DuBois, R. N. (2015). Immunosuppression associated with chronic inflammation in the tumor microenvironment. *Carcinogenesis*, 36(10), 1085–1093. https://doi.org/10.1093/carcin/bgv123

[8] Axelrad, J. E., Lichtiger, S., & Yajnik, V. (2016). Inflammatory bowel disease and cancer: The role of inflammation, immunosuppression, and cancer treatment. *World journal of gastroenterology*, *22*(20), 4794–4801. https://doi.org/10.3748/wjg.v22.i20.4794

[9] Takiguchi, Y., Sekine, I., Iwasawa, S., Kurimoto, R., & Tatsumi, K. (2014). Chronic obstructive pulmonary disease as a risk factor for lung cancer. *World journal of clinical oncology*, 5(4), 660–666. https://doi.org/10.5306/wjco.v5.i4.660

[10] Kandane-Rathnayake, R.K. et al. (2009) Adherence to asthma management guidelines by middle-aged adults with current asthma. *Thorax* 64, 1025–1031

[11] Kuruvilla, M. E., Lee, F. E., & Lee, G. B. (2019). Understanding Asthma Phenotypes, Endotypes, and Mechanisms of Disease. *Clinical reviews in allergy & immunology*, 56(2), 219-233. https://doi.org/10.1007/s12016-018-8712-1

[12] Desai, M., & Oppenheimer, J. (2016). Elucidating asthma phenotypes and endotypes: progress towards personalized medicine. *Annals of allergy, asthma & immunology : official publication of the American College of Allergy, Asthma, & Immunology*, *116*(5), 394–401. https://doi.org/10.1016/j.anai.2015.12.024

[13] Rosenberger, A., Bickeböller, H., McCormack, V., Brenner, D. R., Duell, E. J., Tjønneland,A., Friis, S., Muscat, J. E., Yang, P., Wichmann, H. E., Heinrich, J., Szeszenia-Dabrowska, N., Lissowska, J., Zaridze, D., Rudnai, P., Fabianova, E., Janout, V., Bencko, V., Brennan, P., Mates, D., … Hung, R. J. (2012). Asthma and lung cancer risk: a systematic investigation by the International Lung Cancer Consortium. *Carcinogenesis*, *33*(3), 587–597. https://doi.org/10.1093/carcin/bgr307

[14] Brown, D. W., Young, K. E., Anda, R. F., & Giles, W. H. (2005). Asthma and risk of death from lung cancer: NHANES II Mortality Study. *The Journal of asthma : official journal of the Association for the Care of Asthma*, *42*(7), 597–600. https://doi.org/10.1080/02770900500216234

[15] Qu, Y. L., Liu, J., Zhang, L. X., Wu, C. M., Chu, A. J., Wen, B. L., Ma, C., Yan, X. Y., Zhang, X., Wang, D. M., Lv, X., & Hou, S. J. (2017). Asthma and the risk of lung cancer: a meta-analysis. *Oncotarget*, *8*(7), 11614–11620. https://doi.org/10.18632/oncotarget.14595

[16] Woo, A., Lee, S. W., Koh, H. Y., Kim, M. A., Han, M. Y., & Yon, D. K. (2021). Incidence of cancer after asthma development: 2 independent population-based cohort studies. *The Journal of allergy and clinical immunology*, *147*(1), 135–143. https://doi.org/10.1016/j.jaci.2020.04.041

[17] Gregory, L. G., & Lloyd, C. M. (2011). Orchestrating house dust mite-associated allergy in the lung. *Trends in immunology*, 32(9), 402–411. https://doi.org/10.1016/j.it.2011.06.006

[18] Naylor, M. S., Stamp, G. W., Foulkes, W. D., Eccles, D., & Balkwill, F. R. (1993). Tumor necrosis factor and its receptors in human ovarian cancer. Potential role in disease progression. *The Journal of clinical investigation*, *91*(5), 2194–2206. https://doi.org/10.1172/JCI116446

[19] Mahmutovic Persson, I., Menzel, M., Ramu, S., Cerps, S., Akbarshahi, H., & Uller, L. (2018). IL-1β mediates lung neutrophilia and IL-33 expression in a mouse model of viral-induced asthma exacerbation. *Respiratory research*, *19*(1), 16. https://doi.org/10.1186/s12931-018-0725-z

[20] Rocha, F., Delitto, A. E., de Souza, J., González-Maldonado, L. A., Wallet, S. M., & Rossa Junior, C. (2020). Relevance of Caspase-1 and Nlrp3 Inflammasome on Inflammatory Bone Resorption in A Murine Model of Periodontitis. *Scientific reports*, *10*(1), 7823. https://doi.org/10.1038/s41598-020-64685-y

[21] Kelley, N., Jeltema, D., Duan, Y., & He, Y. (2019). The NLRP3 Inflammasome: An Overview of Mechanisms of Activation and Regulation. *International journal of molecular sciences*, 20(13), 3328. https://doi.org/10.3390/ijms20133328

[22] Franchi, L., Eigenbrod, T., Muñoz-Planillo, R., & Nuñez, G. (2009). The inflammasome: a caspase-1-activation platform that regulates immune responses and disease pathogenesis. Nature immunology, 10(3), 241–247. https://doi.org/10.1038/ni.1703

[23] Woo, L. N., Guo, W. Y., Wang, X., Young, A., Salehi, S., Hin, A., Zhang, Y., Scott, J. A., & Chow, C. W. (2018). A 4-Week Model of House Dust Mite (HDM) Induced Allergic Airways Inflammation with Airway Remodeling. *Scientific reports*, *8*(1), 6925. https://doi.org/10.1038/s41598-018-24574-x

[24] Sousa, A. R., Lane, S. J., Nakhosteen, J. A., Lee, T. H., & Poston, R. N. (1996). Expression of interleukin-1 beta (IL-1beta) and interleukin-1 receptor antagonist (IL-1ra) on asthmatic bronchial epithelium. *American journal of respiratory and critical care medicine*, *154*(4 Pt 1), 1061–1066. https://doi.org/10.1164/ajrccm.154.4.8887608

[25] Gelfo, V., Romaniello, D., Mazzeschi, M., Sgarzi, M., Grilli, G., Morselli, A., Manzan, B., Rihawi, K., & Lauriola, M. (2020). Roles of IL-1 in Cancer: From Tumor Progression to Resistance to Targeted Therapies. *International journal of molecular sciences*, 21(17), 6009. https://doi.org/10.3390/ijms21176009

[26] Choi, Y. H., & Kim, J. K. (2019). Dissecting Cellular Heterogeneity Using Single-Cell RNA Sequencing. *Molecules and cells*, *42*(3), 189–199. https://doi.org/10.14348/molcells.2019.2446

[27] Franks, T. J., Colby, T. V., Travis, W. D., Tuder, R. M., Reynolds, H. Y., Brody, A. R., Cardoso, W. V., Crystal, R. G., Drake, C. J., Engelhardt, J., Frid, M., Herzog, E., Mason, R., Phan, S. H., Randell, S. H., Rose, M. C., Stevens, T., Serge, J., Sunday, M. E., Voynow, J. A., … Williams, M. C. (2008). Resident cellular components of the human lung: current knowledge and goals for research on cell phenotyping and function. *Proceedings of the American Thoracic Society*, *5*(7), 763–766. https://doi.org/10.1513/pats.200803-025HR

[28] Li, H., Cho, S. N., Evans, C. M., Dickey, B. F., Jeong, J. W., & DeMayo, F. J. (2008). Cre-mediated recombination in mouse Clara cells. *Genesis (New York, N.Y. : 2000)*, *46*(6), 300–307. https://doi.org/10.1002/dvg.20396

[29] Moghaddam, S. J., Li, H., Cho, S. N., Dishop, M. K., Wistuba, I. I., Ji, L., Kurie, J. M., Dickey, B. F., & Demayo, F. J. (2009). Promotion of lung carcinogenesis by chronic obstructive pulmonary disease-like airway inflammation in a K-ras-induced mouse model. *American journal of respiratory cell and molecular biology*, *40*(4), 443–453. https://doi.org/10.1165/rcmb.2008-0198OC

[30] Satija, R., Farrell, J. A., Gennert, D., Schier, A. F., & Regev, A. (2015). Spatial reconstruction of single-cell gene expression data. *Nature biotechnology*, *33*(5), 495–502. https://doi.org/10.1038/nbt.3192

[31] Jackson, E. L., Willis, N., Mercer, K., Bronson, R. T., Crowley, D., Montoya, R., Jacks, T., & Tuveson, D. A. (2001). Analysis of lung tumor initiation and progression using conditional expression of oncogenic K-ras. *Genes & development*, *15*(24), 3243–3248. https://doi.org/10.1101/gad.943001

[32] Karan D. (2018). Inflammasomes: Emerging Central Players in Cancer Immunology and Immunotherapy. *Frontiers in immunology*, *9*, 3028. https://doi.org/10.3389/fimmu.2018.03028

[33] Moossavi, M., Parsamanesh, N., Bahrami, A., Atkin, S. L., & Sahebkar, A. (2018). Role of the NLRP3 inflammasome in cancer. *Molecular cancer*, *17*(1), 158. https://doi.org/10.1186/s12943-018-0900-3

[34] Guarda, G., Zenger, M., Yazdi, A. S., Schroder, K., Ferrero, I., Menu, P., Tardivel, A., Mattmann, C., & Tschopp, J. (2011). Differential expression of NLRP3 among hematopoietic cells. *Journal of immunology (Baltimore, Md. : 1950)*, *186*(4), 2529–2534. https://doi.org/10.4049/jimmunol.1002720

[35] Kelley, N., Jeltema, D., Duan, Y., & He, Y. (2019). The NLRP3 Inflammasome: An Overview of Mechanisms of Activation and Regulation. *International journal of molecular sciences*, *20*(13), 3328. https://doi.org/10.3390/ijms20133328

[36] Deshmane, S. L., Kremlev, S., Amini, S., & Sawaya, B. E. (2009). Monocyte chemoattractant protein-1 (MCP-1): an overview. *Journal of interferon & cytokine research : the official journal of the International Society for Interferon and Cytokine Research*, *29*(6), 313–326. https://doi.org/10.1089/jir.2008.0027

[37] Ji, H., Houghton, A. M., Mariani, T. J., Perera, S., Kim, C. B., Padera, R., Tonon, G., McNamara, K., Marconcini, L. A., Hezel, A., El-Bardeesy, N., Bronson, R. T., Sugarbaker, D., Maser, R. S., Shapiro, S. D., & Wong, K. K. (2006). K-ras activation generates an inflammatory response in lung tumors. *Oncogene*, *25*(14), 2105–2112. https://doi.org/10.1038/sj.onc.1209237

[38] McLoed, A. G., Sherrill, T. P., Cheng, D. S., Han, W., Saxon, J. A., Gleaves, L. A., Wu, P., Polosukhin, V. V., Karin, M., Yull, F. E., Stathopoulos, G. T., Georgoulias, V., Zaynagetdinov, R., & Blackwell, T. S. (2016). Neutrophil-Derived IL-1β Impairs the Efficacy of NF-κB Inhibitors against Lung Cancer. Cell reports, 16(1), 120–132. https://doi.org/10.1016/j.celrep.2016.05.085

[39] Meuwissen, R., & Berns, A. (2005). Mouse models for human lung cancer. *Genes & development*, *19*(6), 643–664. https://doi.org/10.1101/gad.1284505

[40] Tuveson, D. A., & Jacks, T. (1999). Modeling human lung cancer in mice: similarities and shortcomings. *Oncogene*, *18*(38), 5318–5324. https://doi.org/10.1038/sj.onc.1203107

[41] Miller, Y. E., Dwyer-Nield, L. D., Keith, R. L., Le, M., Franklin, W. A., & Malkinson, A. M. (2003). Induction of a high incidence of lung tumors in C57BL/6 mice with multiple ethyl carbamate injections. *Cancer letters*, 198(2), 139–144. https://doi.org/10.1016/s0304-3835(03)00309-4

[42] Becht, E., McInnes, L., Healy, J., Dutertre, C. A., Kwok, I., Ng, L. G., Ginhoux, F., & Newell, E. W. (2018). Dimensionality reduction for visualizing single-cell data using UMAP. Nature biotechnology, 10.1038/nbt.4314. *Advance online publication*. https://doi.org/10.1038/nbt.4314

[43] Aran, D., Looney, A. P., Liu, L., Wu, E., Fong, V., Hsu, A., Chak, S., Naikawadi, R. P., Wolters, P. J., Abate, A. R., Butte, A. J., & Bhattacharya, M. (2019). Reference-based analysis of lung single-cell sequencing reveals a

transitional profibrotic macrophage. Nature immunology, 20(2), 163–172. https://doi.org/10.1038/s41590-018-0276-y

[44] Zemmour, D., Zilionis, R., Kiner, E., Klein, A. M., Mathis, D., & Benoist, C. (2018). Single-cell gene expression reveals a landscape of regulatory T cell phenotypes shaped by the TCR. *Nature immunology*, *19*(3), 291–301. https://doi.org/10.1038/s41590-018-0051-0

[45] Shevyrev, D., & Tereshchenko, V. (2020). Treg Heterogeneity, Function, and Homeostasis. *Frontiers in immunology*, *10*, 3100. https://doi.org/10.3389/fimmu.2019.03100

[46] Kannan, A. K., Su, Z., Gauvin, D. M., Paulsboe, S. E., Duggan, R., Lasko, L. M., Honore, P., Kort, M. E., McGaraughty, S. P., Scott, V. E., & Gauld, S. B. (2019). IL-23 induces regulatory T cell plasticity with implications for inflammatory skin diseases. *Scientific reports*, 9(1), 17675. https://doi.org/10.1038/s41598-019-53240-z

[47] Sakaguchi, S., Vignali, D. A., Rudensky, A. Y., Niec, R. E., & Waldmann, H. (2013). The plasticity and stability of regulatory T cells. Nature reviews. Immunology, 13(6), 461–467. https://doi.org/10.1038/nri3464

[48] Vaeth, M., Wang, Y. H., Eckstein, M., Yang, J., Silverman, G. J., Lacruz, R. S., Kannan, K., & Feske, S. (2019). Tissue resident and follicular Treg cell differentiation is regulated by CRAC channels. Nature communications, 10(1), 1183. https://doi.org/10.1038/s41467-019-08959-8

[49] Neumann, C., Blume, J., Roy, U., Teh, P. P., Vasanthakumar, A., Beller, A., Liao, Y., Heinrich, F., Arenzana, T. L., Hackney, J. A., Eidenschenk, C., Gálvez, E., Stehle, C., Heinz, G. A., Maschmeyer, P., Sidwell, T., Hu, Y., Amsen, D., Romagnani, C., Chang, H. D., … Scheffold, A. (2019). c-Maf-dependent T_{reg} cell control of intestinal T_H17 cells and IgA establishes host-microbiota homeostasis. *Nature immunology*, *20*(4), 471–481. https://doi.org/10.1038/s41590-019-0316-2

[50] Li, L., Kim, J., & Boussiotis, V. A. (2010). IL-1β-mediated signals preferentially drive conversion of regulatory T cells but not conventional T cells into IL-17-producing cells. *Journal of immunology (Baltimore, Md. : 1950)*, *185*(7), 4148–4153. https://doi.org/10.4049/jimmunol.1001536

[51] Wang, W., Xiang, L., Liu, Y. G., Wang, Y. H., & Shen, K. L. (2010). Effect of house dust mite immunotherapy on interleukin-10-secreting regulatory T cells in asthmatic children. *Chinese medical journal*, *123*(15), 2099–2104.

[52] Böttcher, J. P., Beyer, M., Meissner, F., Abdullah, Z., Sander, J., Höchst, B., Eickhoff, S., Rieckmann, J. C., Russo, C., Bauer, T., Flecken, T., Giesen, D., Engel, D., Jung, S., Busch, D. H., Protzer, U., Thimme, R., Mann, M., Kurts, C., Schultze, J. L., … Knolle, P. A. (2015). Functional classification of memory CD8(+) T cells by CX3CR1 expression. *Nature communications*, *6*, 8306. https://doi.org/10.1038/ncomms9306

[53] Omilusik, K. D., Best, J. A., Yu, B., Goossens, S., Weidemann, A., Nguyen, J. V., Seuntjens, E., Stryjewska, A., Zweier, C., Roychoudhuri, R., Gattinoni, L., Bird, L. M., Higashi, Y., Kondoh, H., Huylebroeck, D., Haigh, J., & Goldrath, A. W. (2015). Transcriptional repressor ZEB2 promotes terminal differentiation of CD8+ effector and memory T cell populations during infection. *The Journal of experimental medicine*, *212*(12), 2027–2039. https://doi.org/10.1084/jem.20150194

[54] Bachmann, M. F., Wolint, P., Schwarz, K., Jäger, P., & Oxenius, A. (2005). Functional properties and lineage relationship of CD8+ T cell subsets identified by expression of IL-7 receptor alpha and CD62L. *Journal of immunology (Baltimore, Md. : 1950)*, *175*(7), 4686–4696. https://doi.org/10.4049/jimmunol.175.7.4686

[55] Weatherly, K., Bettonville, M., Torres, D., Kohler, A., Goriely, S., & Braun, M. Y. (2015). Functional profile of S100A4-deficient T cells. *Immunity, inflammation and disease*, *3*(4), 431–444. https://doi.org/10.1002/iid3.85

[56] Drujont, L., Lemoine, A., Moreau, A., Bienvenu, G., Lancien, M., Cens, T., Guillot, F., Bériou, G., Bouchet-Delbos, L., Fehling, H. J., Chiffoleau, E., Nicot, A. B., Charnet, P., Martin, J. C., Josien, R., Cuturi, M. C., & Louvet, C. (2016). RORγt+ cells selectively express redundant cation channels linked to the Golgi apparatus. *Scientific reports*, *6*, 23682. https://doi.org/10.1038/srep23682

[57] Tan, L., Sandrock, I., Odak, I., Aizenbud, Y., Wilharm, A., Barros-Martins, J., Tabib, Y., Borchers, A., Amado, T., Gangoda, L., Herold, M. J., Schmidt-Supprian, M., Kisielow, J., Silva-Santos, B., Koenecke, C., Hovav, A. H., Krebs, C., Prinz, I., & Ravens, S. (2019). Single-Cell Transcriptomics Identifies the Adaptation of Scart1^{+} Vγ6^{+} T Cells to Skin Residency as Activated Effector Cells. *Cell reports*, *27*(12), 3657–3671.e4. https://doi.org/10.1016/j.celrep.2019.05.064

[58] Haim-Vilmovsky, L., Henriksson, J., Walker, J. A., Miao, Z., Natan, E., Kar, G., Clare, S., Barlow, J. L., Charidemou, E., Mamanova, L., Chen, X., Proserpio, V., Pramanik, J., Woodhouse, S., Protasio, A. V., Efremova, M., Griffin, J. L., Berriman, M., Dougan, G., Fisher, J., … Teichmann, S. A. (2021). Mapping Rora expression in resting and activated CD4+ T cells. *PloS one*, 16(5), e0251233. https://doi.org/10.1371/journal.pone.0251233

[59] Hwang, S. H., Jung, S. H., Lee, S., Choi, S., Yoo, S. A., Park, J. H., Hwang, D., Shim, S. C., Sabbagh, L., Kim, K. J., Park, S. H., Cho, C. S., Kim, B. S., Leng, L., Montgomery, R. R., Bucala, R., Chung, Y. J., & Kim, W. U. (2015). Leukocyte-specific protein 1 regulates T-cell migration in rheumatoid arthritis. *Proceedings of the National Academy of Sciences of the United States of America*, *112*(47), E6535–E6543. https://doi.org/10.1073/pnas.1514152112

[60] Lin, C. C., Bradstreet, T. R., Schwarzkopf, E. A., Sim, J., Carrero, J. A., Chou, C., Cook, L. E., Egawa, T., Taneja, R., Murphy, T. L., Russell, J. H., & Edelson, B. T. (2014). Bhlhe40 controls cytokine production by T cells and is essential for pathogenicity in autoimmune neuroinflammation. *Nature communications*, 5, 3551. https://doi.org/10.1038/ncomms4551

[61] Wilson, A. N., Mosure, S. A., & Solt, L. A. (2022). A Compass to Guide Insights into T_H17 Cellular Metabolism and Autoimmunity. *Immunometabolism*, *4*(1), e220001. https://doi.org/10.20900/immunometab20220001

[62] Bortnick, A., He, Z., Aubrey, M., Chandra, V., Denholtz, M., Chen, K., Lin, Y. C., & Murre, C. (2020). Plasma Cell Fate Is Orchestrated by Elaborate Changes in Genome Compartmentalization and Inter-chromosomal Hubs. Cell reports, 31(1), 107470. https://doi.org/10.1016/j.celrep.2020.03.034

[63] Zhu, Y. X., Benn, S., Li, Z. H., Wei, E., Masih-Khan, E., Trieu, Y., Bali, M., McGlade, C. J., Claudio, J. O., & Stewart, A. K. (2004). The SH3-SAM adaptor HACS1 is up-regulated in B cell activation signaling cascades. *The Journal of experimental medicine*, *200*(6), 737–747. https://doi.org/10.1084/jem.20031816

[64] Ruiz-Lafuente, N., Minguela, A., Muro, M., & Parrado, A. (2019). The role of DOCK10 in the regulation of the transcriptome and aging. *Heliyon*, 5(3), e01391. https://doi.org/10.1016/j.heliyon.2019.e01391

[65] Wiede, F., Fromm, P. D., Comerford, I., Kara, E., Bannan, J., Schuh, W., Ranasinghe, C., Tarlinton, D., Winkler, T., McColl, S. R., & Körner, H. (2013). CCR6 is transiently upregulated on B cells after activation and modulates the germinal center reaction in the mouse. *Immunology and cell biology*, *91*(5), 335–339. https://doi.org/10.1038/icb.2013.14

[66] Tang, H., Chen, J., Han, X., Feng, Y., & Wang, F. (2021). Upregulation of *SPP1* Is a Marker for Poor Lung Cancer Prognosis and Contributes to Cancer Progression and Cisplatin Resistance. *Frontiers in cell and developmental biology*, *9*, 646390. https://doi.org/10.3389/fcell.2021.646390

[67] Watanabe, K., Jose, P. J., & Rankin, S. M. (2002). Eotaxin-2 generation is differentially regulated by lipopolysaccharide and IL-4 in monocytes and macrophages. *Journal of immunology (Baltimore, Md. : 1950)*, *168*(4), 1911–1918. https://doi.org/10.4049/jimmunol.168.4.1911

[68] Li, B., Zhang, S., Huang, N., Chen, H., Wang, P., Yang, J., & Li, Z. (2019). CCL9/CCR1 induces myeloid-derived suppressor cell recruitment to the spleen in a murine H22 orthotopic hepatoma model. *Oncology reports*, *41*(1), 608–618. https://doi.org/10.3892/or.2018.6809

[69] Zakrzewicz, A., Richter, K., Zakrzewicz, D., Siebers, K., Damm, J., Agné, A., Hecker, A., McIntosh, J. M., Chamulitrat, W., Krasteva-Christ, G., Manzini, I., Tikkanen, R., Padberg, W., Janciauskiene, S., & Grau, V. (2019).

SLPI Inhibits ATP-Mediated Maturation of IL-1β in Human Monocytic Leukocytes: A Novel Function of an Old Player. *Frontiers in immunology*, *10*, 664. https://doi.org/10.3389/fimmu.2019.00664

[70] Zakrzewicz, A., Richter, K., Zakrzewicz, D., Siebers, K., Damm, J., Agné, A., Hecker, A., McIntosh, J. M., Chamulitrat, W., Krasteva-Christ, G., Manzini, I., Tikkanen, R., Padberg, W., Janciauskiene, S., & Grau, V. (2019). SLPI Inhibits ATP-Mediated Maturation of IL-1β in Human Monocytic Leukocytes: A Novel Function of an Old Player. *Frontiers in immunology*, *10*, 664. https://doi.org/10.3389/fimmu.2019.00664

[71] Sedighzadeh, S. S., Khoshbin, A. P., Razi, S., Keshavarz-Fathi, M., & Rezaei, N. (2021). A narrative review of tumor-associated macrophages in lung cancer: regulation of macrophage polarization and therapeutic implications. *Translational lung cancer research*, *10*(4), 1889–1916. https://doi.org/10.21037/tlcr-20-1241

[72] Prince, L. R., Allen, L., Jones, E. C., Hellewell, P. G., Dower, S. K., Whyte, M. K., & Sabroe, I. (2004). The role of interleukin-1beta in direct and toll-like receptor 4-mediated neutrophil activation and survival. *The American journal of pathology*, *165*(5), 1819–1826. https://doi.org/10.1016/s0002-9440(10)63437-2

[73] Meher, A. K., Spinosa, M., Davis, J. P., Pope, N., Laubach, V. E., Su, G., Serbulea, V., Leitinger, N., Ailawadi, G., & Upchurch, G. R., Jr (2018). Novel Role of IL (Interleukin)-1β in Neutrophil Extracellular Trap Formation and Abdominal Aortic Aneurysms. *Arteriosclerosis, thrombosis, and vascular biology*, *38*(4), 843–853. https://doi.org/10.1161/ATVBAHA.117.309897

[74] Rosales C. (2018). Neutrophil: A Cell with Many Roles in Inflammation or Several Cell Types?. *Frontiers in physiology*, *9*, 113. https://doi.org/10.3389/fphys.2018.00113

[75] Stockfelt, M., Christenson, K., Andersson, A., Björkman, L., Padra, M., Brundin, B., Ganguly, K., Asgeirsdottir, H., Lindén, S., Qvarfordt, I., Bylund, J., & Lindén, A. (2020). Increased CD11b and Decreased CD62L in Blood and Airway Neutrophils from Long-Term Smokers with and without COPD. *Journal of innate immunity*, *12*(6), 480–489. https://doi.org/10.1159/000509715

[76] Woodfin, A., Reichel, C. A., Khandoga, A., Corada, M., Voisin, M. B., Scheiermann, C., Haskard, D. O., Dejana, E., Krombach, F., & Nourshargh, S. (2007). JAM-A mediates neutrophil transmigration in a stimulus-specific manner in vivo: evidence for sequential roles for JAM-A and PECAM-1 in neutrophil transmigration. *Blood*, *110*(6), 1848–1856. https://doi.org/10.1182/blood-2006-09-047431

[77] Calcagno, D. M., Zhang, C., Toomu, A., Huang, K., Ninh, V. K., Miyamoto, S., Aguirre, A. D., Fu, Z., Heller Brown, J., & King, K. R. (2021). SiglecF(HI) Marks Late-Stage Neutrophils of the Infarcted Heart: A Single-Cell Transcriptomic Analysis of Neutrophil Diversification. *Journal of the American Heart Association*, *10*(4), e019019. https://doi.org/10.1161/JAHA.120.019019

[78] Puellmann, K., Kaminski, W. E., Vogel, M., Nebe, C. T., Schroeder, J., Wolf, H., & Beham, A. W. (2006). A variable immunoreceptor in a subpopulation of human neutrophils. *Proceedings of the National Academy of Sciences of the United States of America*, *103*(39), 14441–14446. https://doi.org/10.1073/pnas.0603406103

[79] Melissa A. Meyer, Huy Q. Dinh, Yanfang Zhu, Shu Liang, Gregory Seumois, Pandurangan Vijayanand, Sergio D. Catz, Catherine C. Hedrick. (2020). Abstract 3311: B cell like neutrophil found in peripheral blood of melanoma patients. *Cancer Res* 15, 80 (16_Supplement): 3311. https://doi.org/10.1158/1538-7445.AM2020-3311

[80] Tsou, C. L., Peters, W., Si, Y., Slaymaker, S., Aslanian, A. M., Weisberg, S. P., Mack, M., & Charo, I. F. (2007). Critical roles for CCR2 and MCP-3 in monocyte mobilization from bone marrow and recruitment to inflammatory sites. *The Journal of clinical investigation*, *117*(4), 902–909. https://doi.org/10.1172/JCI29919

[81] França, C. N., Izar, M., Hortêncio, M., do Amaral, J. B., Ferreira, C., Tuleta, I. D., & Fonseca, F. (2017). Monocyte subtypes and the CCR2 chemokine receptor in cardiovascular disease. *Clinical science (London, England : 1979)*, *131*(12), 1215–1224. https://doi.org/10.1042/CS20170009

[82] Walker L. S. (2013). Treg and CTLA-4: two intertwining pathways to immune tolerance. Journal of autoimmunity, 45(100), 49–57. https://doi.org/10.1016/j.jaut.2013.06.006

[83] Tang, Q., & Krummel, M. F. (2006). Imaging the function of regulatory T cells in vivo. *Current opinion in immunology*, *18*(4), 496–502. https://doi.org/10.1016/j.coi.2006.05.007

[84] Carmenate, T., Ortíz, Y., Enamorado, M., García-Martínez, K., Avellanet, J., Moreno, E., Graça, L., & León, K. (2018). Blocking IL-2 Signal In Vivo with an IL-2 Antagonist Reduces Tumor Growth through the Control of Regulatory T Cells. *Journal of immunology (Baltimore, Md. : 1950)*, *200*(10), 3475–3484. https://doi.org/10.4049/jimmunol.1700433

[85] Beriou, G., Costantino, C. M., Ashley, C. W., Yang, L., Kuchroo, V. K., Baecher-Allan, C., & Hafler, D. A. (2009). IL-17-producing human peripheral regulatory T cells retain suppressive function. *Blood*, *113*(18), 4240–4249. https://doi.org/10.1182/blood-2008-10-183251

[86] Tanaka, A., & Sakaguchi, S. (2017). Regulatory T cells in cancer immunotherapy. *Cell research*, *27*(1), 109–118. https://doi.org/10.1038/cr.2016.151

[87] Parga-Vidal, L., & van Gisbergen, K. (2020). Area under Immunosurveillance: Dedicated Roles of Memory CD8 T-Cell Subsets. *Cold Spring Harbor perspectives in biology*, *12*(11), a037796. https://doi.org/10.1101/cshperspect.a037796

[88] Reiser, J., & Banerjee, A. (2016). Effector, Memory, and Dysfunctional CD8(+) T Cell Fates in the Antitumor Immune Response. *Journal of immunology research*, *2016*, 8941260. https://doi.org/10.1155/2016/8941260

[89] Sakaguchi S. (2004). Naturally arising CD4+ regulatory t cells for immunologic self-tolerance and negative control of immune responses. *Annual review of immunology*, *22*, 531–562. https://doi.org/10.1146/annurev.immunol.21.120601.141122

[90] Tibbitt, C. A., Stark, J. M., Martens, L., Ma, J., Mold, J. E., Deswarte, K., Oliynyk, G., Feng, X., Lambrecht, B. N., De Bleser, P., Nylén, S., Hammad, H., Arsenian Henriksson, M., Saeys, Y., & Coquet, J. M. (2019). Single-Cell RNA Sequencing of the T Helper Cell Response to House Dust Mites Defines a Distinct Gene Expression Signature in Airway Th2 Cells. *Immunity*, *51*(1), 169–184.e5. https://doi.org/10.1016/j.immuni.2019.05.014

[91] Krishnamoorthy, N., Douda, D. N., Brüggemann, T. R., Ricklefs, I., Duvall, M. G., Abdulnour, R. E., Martinod, K., Tavares, L., Wang, X., Cernadas, M., Israel, E., Mauger, D. T., Bleecker, E. R., Castro, M., Erzurum, S. C., Gaston, B. M., Jarjour, N. N., Wenzel, S., Dunican, E., Fahy, J. V., … National Heart, Lung, and Blood Institute Severe Asthma Research Program-3 Investigators (2018). Neutrophil cytoplasts induce T_H17 differentiation and skew inflammation toward neutrophilia in severe asthma. *Science immunology*, *3*(26), eaao4747. https://doi.org/10.1126/sciimmunol.aao4747

[92] Joerger, M., Finn, S. P., Cuffe, S., Byrne, A. T., & Gray, S. G. (2016). The IL-17-Th1/Th17 pathway: an attractive target for lung cancer therapy?. *Expert opinion on therapeutic targets*, *20*(11), 1339–1356. https://doi.org/10.1080/14728222.2016.1206891

[93] Marshall, E. A., Ng, K. W., Kung, S. H., Conway, E. M., Martinez, V. D., Halvorsen, E. C., Rowbotham, D. A., Vucic, E. A., Plumb, A. W., Becker-Santos, D. D., Enfield, K. S., Kennett, J. Y., Bennewith, K. L., Lockwood, W. W., Lam, S., English, J. C., Abraham, N., & Lam, W. L. (2016). Emerging roles of T helper 17 and regulatory T cells in lung cancer progression and metastasis. *Molecular cancer*, *15*(1), 67. https://doi.org/10.1186/s12943-016-0551-1

[94] Wu, F., Xu, J., Huang, Q., Han, J., Duan, L., Fan, J., Lv, Z., Guo, M., Hu, G., Chen, L., Zhang, S., Tao, X., Ma, W., & Jin, Y. (2016). The Role of Interleukin-17 in Lung Cancer. *Mediators of inflammation*, *2016*, 8494079. https://doi.org/10.1155/2016/8494079

[95] Chen, X., Wan, J., Liu, J., Xie, W., Diao, X., Xu, J., Zhu, B., & Chen, Z. (2010). Increased IL-17-producing cells correlate with poor survival and lymphangiogenesis in NSCLC patients. *Lung cancer (Amsterdam, Netherlands)*, *69*(3), 348–354. https://doi.org/10.1016/j.lungcan.2009.11.013

[96] Mailer, R. K., Joly, A. L., Liu, S., Elias, S., Tegner, J., & Andersson, J. (2015). IL-1β promotes Th17 differentiation by inducing alternative splicing of FOXP3. *Scientific reports*, *5*, 14674. https://doi.org/10.1038/srep14674

[97] Li, Q., Han, Y., Fei, G., Guo, Z., Ren, T., & Liu, Z. (2012). IL-17 promoted metastasis of non-small-cell lung cancer cells. *Immunology letters*, *148*(2), 144–150. https://doi.org/10.1016/j.imlet.2012.10.011

[98] Silvestre-Roig, C., Hidalgo, A., & Soehnlein, O. (2016). Neutrophil heterogeneity: implications for homeostasis and pathogenesis. *Blood*, *127*(18), 2173–2181. https://doi.org/10.1182/blood-2016-01-688887

[99] Pillay, J., den Braber, I., Vrisekoop, N., Kwast, L. M., de Boer, R. J., Borghans, J. A., Tesselaar, K., & Koenderman, L. (2010). In vivo labeling with 2H2O reveals a human neutrophil lifespan of 5.4 days. *Blood*, *116*(4), 625–627. https://doi.org/10.1182/blood-2010-01-259028

[100] Martin, C., Burdon, P. C., Bridger, G., Gutierrez-Ramos, J. C., Williams, T. J., & Rankin, S. M. (2003). Chemokines acting via CXCR2 and CXCR4 control the release of neutrophils from the bone marrow and their return following senescence. *Immunity*, *19*(4), 583–593. https://doi.org/10.1016/s1074-7613(03)00263-2

[101] Pfirschke, C., Engblom, C., Gungabeesoon, J., Lin, Y., Rickelt, S., Zilionis, R., Messemaker, M., Siwicki, M., Gerhard, G. M., Kohl, A., Meylan, E., Weissleder, R., Klein, A. M., & Pittet, M. J. (2020). Tumor-Promoting Ly-6G^{+} SiglecF^{high} Cells Are Mature and Long-Lived Neutrophils. *Cell reports*, *32*(12), 108164. https://doi.org/10.1016/j.celrep.2020.108164

[102] Wu, Y., Li, Y. Y., Matsushima, K., Baba, T., & Mukaida, N. (2008). CCL3-CCR5 axis regulates intratumoral accumulation of leukocytes and fibroblasts and promotes angiogenesis in murine lung metastasis process. *Journal of immunology (Baltimore, Md. : 1950)*, *181*(9), 6384–6393. https://doi.org/10.4049/jimmunol.181.9.6384

[103] Li, L., Liu, Y. D., Zhan, Y. T., Zhu, Y. H., Li, Y., Xie, D., & Guan, X. Y. (2018). High levels of CCL2 or CCL4 in the tumor microenvironment predict unfavorable survival in lung adenocarcinoma. *Thoracic cancer*, *9*(7), 775–784. https://doi.org/10.1111/1759-7714.12643

[104] Wightman, S. C., Uppal, A., Pitroda, S. P., Ganai, S., Burnette, B., Stack, M., Oshima, G., Khan, S., Huang, X., Posner, M. C., Weichselbaum, R. R., & Khodarev, N. N. (2015). Oncogenic CXCL10 signalling drives metastasis development and poor clinical outcome. *British journal of cancer*, *113*(2), 327–335. https://doi.org/10.1038/bjc.2015.193

[105] Gong, K., Guo, G., Beckley, N., Zhang, Y., Yang, X., Sharma, M., & Habib, A. A. (2021). Tumor necrosis factor in lung cancer: Complex roles in biology and resistance to treatment. *Neoplasia (New York, N.Y.)*, *23*(2), 189–196. https://doi.org/10.1016/j.neo.2020.12.006

[106] Liu, K., Huang, H. H., Yang, T., Jiao, Y. M., Zhang, C., Song, J. W., Zhang, J. Y., Zhou, C. B., Yuan, J. H., Cao, W. J., Mu, X. Y., Zhou, M. J., Li, H. J., Shi, M., Xu, R., & Wang, F. S. (2021). Increased Neutrophil Aging Contributes to T Cell Immune Suppression by PD-L1 and Arginase-1 in HIV-1 Treatment Naïve Patients. *Frontiers in immunology*, *12*, 670616. https://doi.org/10.3389/fimmu.2021.670616

[107] Hassane, M., Demon, D., Soulard, D., Fontaine, J., Keller, L. E., Patin, E. C., Porte, R., Prinz, I., Ryffel, B., Kadioglu, A., Veening, J. W., Sirard, J. C., Faveeuw, C., Lamkanfi, M., Trottein, F., & Paget, C. (2017). Neutrophilic NLRP3 inflammasome-dependent IL-1β secretion regulates the γδT17 cell response in respiratory bacterial infections. *Mucosal immunology*, *10*(4), 1056–1068. https://doi.org/10.1038/mi.2016.113

[108] Cho, J. S., Guo, Y., Ramos, R. I., Hebroni, F., Plaisier, S. B., Xuan, C., Granick, J. L., Matsushima, H., Takashima, A., Iwakura, Y., Cheung, A. L., Cheng, G., Lee, D. J., Simon, S. I., & Miller, L. S. (2012). Neutrophil-

derived IL-1β is sufficient for abscess formation in immunity against Staphylococcus aureus in mice. *PLoS pathogens*, *8*(11), e1003047. https://doi.org/10.1371/journal.ppat.1003047

[109] Hu, Q., Shi, H., Zeng, T., Liu, H., Su, Y., Cheng, X., Ye, J., Yin, Y., Liu, M., Zheng, H., Wu, X., Chi, H., Zhou, Z., Jia, J., Sun, Y., Teng, J., & Yang, C. (2019). Increased neutrophil extracellular traps activate NLRP3 and inflammatory macrophages in adult-onset Still's disease. *Arthritis research & therapy*, *21*(1), 9. https://doi.org/10.1186/s13075-018-1800-z

[110] Monteith, A. J., Miller, J. M., Maxwell, C. N., Chazin, W. J., & Skaar, E. P. (2021). Neutrophil extracellular traps enhance macrophage killing of bacterial pathogens. *Science advances*, *7*(37), eabj2101. https://doi.org/10.1126/sciadv.abj2101

[111] Masucci, M. T., Minopoli, M., Del Vecchio, S., & Carriero, M. V. (2020). The Emerging Role of Neutrophil Extracellular Traps (NETs) in Tumor Progression and Metastasis. *Frontiers in immunology*, *11*, 1749. https://doi.org/10.3389/fimmu.2020.01749

[112] Sedighzadeh, S. S., Khoshbin, A. P., Razi, S., Keshavarz-Fathi, M., & Rezaei, N. (2021). A narrative review of tumor-associated macrophages in lung cancer: regulation of macrophage polarization and therapeutic implications. *Translational lung cancer research*, *10*(4), 1889–1916. https://doi.org/10.21037/tlcr-20-1241

[113] Parisi, L., Gini, E., Baci, D., Tremolati, M., Fanuli, M., Bassani, B., Farronato, G., Bruno, A., & Mortara, L. (2018). Macrophage Polarization in Chronic Inflammatory Diseases: Killers or Builders?. *Journal of immunology research*, *2018*, 8917804. https://doi.org/10.1155/2018/8917804

[114] Liu, Y., Gao, X., Miao, Y., Wang, Y., Wang, H., Cheng, Z., Wang, X., Jing, X., Jia, L., Dai, L., Liu, M., & An, L. (2018). NLRP3 regulates macrophage M2 polarization through up-regulation of IL-4 in asthma. *The Biochemical journal*, *475*(12), 1995–2008. https://doi.org/10.1042/BCJ20180086

[115] Ridker, P. M., MacFadyen, J. G., Thuren, T., Everett, B. M., Libby, P., Glynn, R. J., & CANTOS Trial Group (2017). Effect of interleukin-1β inhibition with canakinumab on incident lung cancer in patients with atherosclerosis: exploratory results from a randomised, double-blind, placebo-controlled trial. *Lancet (London, England)*, *390*(10105), 1833–1842. https://doi.org/10.1016/S0140-6736(17)32247-X

[116] Wong, C. C., Baum, J., Silvestro, A., Beste, M. T., Bharani-Dharan, B., Xu, S., Wang, Y. A., Wang, X., Prescott, M. F., Krajkovich, L., Dugan, M., Ridker, P. M., Martin, A. M., & Svensson, E. C. (2020). Inhibition of IL1β by Canakinumab May Be Effective against Diverse Molecular Subtypes of Lung Cancer: An Exploratory Analysis of the CANTOS Trial. *Cancer research*, *80*(24), 5597–5605. https://doi.org/10.1158/0008-5472.CAN-19-3176

[117] Sierra-Filardi, E., Nieto, C., Domínguez-Soto, A., Barroso, R., Sánchez-Mateos, P., Puig-Kroger, A., López-Bravo, M., Joven, J., Ardavín, C., Rodríguez-Fernández, J. L., Sánchez-Torres, C., Mellado, M., & Corbí, A. L. (2014). CCL2 shapes macrophage polarization by GM-CSF and M-CSF: identification of CCL2/CCR2-dependent gene expression profile. *Journal of immunology (Baltimore, Md. : 1950)*, *192*(8), 3858–3867. https://doi.org/10.4049/jimmunol.1302821

[118] Zhao, S., Zheng, X., Zhu, X., Ning, J., Zhu, K., Yan, Y., Zhang, J., Bu, J., Liu, M., & Xu, S. (2022). Surgical Trauma-induced CCL2 Upregulation Mediates Lung Cancer Progression by Promoting Treg Recruitment in Mice and Patients. *Cancer investigation*, *40*(2), 91–102. https://doi.org/10.1080/07357907.2021.1977314

[119] Wang, L., Netto, K. G., Zhou, L., Liu, X., Wang, M., Zhang, G., Foster, P. S., Li, F., & Yang, M. (2021). Single-cell transcriptomic analysis reveals the immune landscape of lung in steroid-resistant asthma exacerbation. *Proceedings of the National Academy of Sciences of the United States of America*, *118*(2), e2005590118. https://doi.org/10.1073/pnas.2005590118

[120] Hurskainen, M., Mižíková, I., Cook, D. P., Andersson, N., Cyr-Depauw, C., Lesage, F., Helle, E., Renesme, L., Jankov, R. P., Heikinheimo, M., Vanderhyden, B. C., & Thébaud, B. (2021). Single cell transcriptomic analysis of

murine lung development on hyperoxia-induced damage. Nature communications, 12(1), 1565. https://doi.org/10.1038/s41467-021-21865-2

[121] De Alba, J., Raemdonck, K., Dekkak, A., Collins, M., Wong, S., Nials, A. T., Knowles, R. G., Belvisi, M. G., & Birrell, M. A. (2010). House dust mite induces direct airway inflammation in vivo: implications for future disease therapy?. *The European respiratory journal*, *35*(6), 1377–1387. https://doi.org/10.1183/09031936.00022908

[122] Piyadasa, H., Altieri, A., Basu, S., Schwartz, J., Halayko, A. J., & Mookherjee, N. (2016). Biosignature for airway inflammation in a house dust mite-challenged murine model of allergic asthma. *Biology open*, *5*(2), 112–121. https://doi.org/10.1242/bio.014464